Self-adjoint eigenvalue problems with low rank perturbations.

Thomas J. Anastasio* Andrea K. Barreiro† Jared C. Bronski‡

May 20, 2017

Abstract

We consider the problem of finding the spectrum of an operator taking the form of a low-rank (rank one or two) non-normal perturbation of a self-adjoint operator, motivated by a number of problems of applied interest which take this form. We use the fact that the system is a low rank perturbation of a symmetric problem, together with a simple idea of classical differential geometry (the envelope of a family of curves) to completely analyze the spectrum of this type of operator. We use these techniques to analyze three problems of this form: a model of the oculomotor integrator due to Anastasio and Gad[1], a continuum integrator model, and a nonlocal model of phase separation due to Rubinstein and Sternberg[2].

Keywords: Bifurcation theory, Aronszajn-Krein formula, Rank one perturbations

1 Introduction and Basic Calculations

In this paper we analyze eigenvalue problems of the following form

$$\widetilde{\mathbf{M}}\vec{w} = \mathbf{M}\vec{w} + \rho_1 \vec{f}_1 \langle \vec{g}_1, \vec{w} \rangle + \rho_2 \vec{f}_2 \langle \vec{g}_2, \vec{w} \rangle = \lambda \vec{w} \tag{1}$$

with ρ_1 and ρ_2 parameters, $\vec{f}_i, \vec{g}_i$ fixed vectors and $\mathbf{M}$ is a self-adjoint operator. While Eqn. 1 might appear very specific, we are aware of a number of interesting eigenvalue problems which take this form. These include:

- A model due to Anastasio and Gad of the behavior of the oculomotor integrator[1].
- A non-local Allen-Cahn model due to Rubinstein and Sternberg for phase separation[2].
- The stability problem for spike solutions to activator-inhibitor models in the limit of slow activator diffusion[3, 4].
- Stability for models of runaway ohmic heating[5, 6, 7] and microwave heating [8].
- Stability for stationary solutions of model for phytoplankton growth.[9]

*Department of Molecular and Integrative Physiology and Beckman Institute, University of Illinois Urbana-Champaign, Urbana, IL 61820.

†Department of Mathematics, Southern Methodist University, Box 750156, Dallas, TX 75275

‡Department of Mathematics, University of Illinois Urbana-Champaign, 1409 W. Green St., Urbana, IL 61801.

Four of the models take the form of a reaction-diffusion equation with a nonlocal term. The study of the stability of stationary solutions to such models naturally leads to an eigenvalue problem in the form of a self-adjoint Sturm-Liouville operator plus a finite rank perturbation coming from the nonlocal term. Freitas[3] has considered a similar problem and has some related results for a single perturbation (rather than a two parameter family); Bose and Kriegsmann[8] have some other related results, mainly in the case where $\vec{f_i} = \vec{g}_i$ where the problem is self-adjoint.

In all of these problems the eigenvalue problem arises in the study of the stability of a particular steady state. In this situation one is typically interested in understanding qualitative properties of the spectrum as a function of the parameters (ρ_1, ρ_2). In particular one might wish to understand, for any particular pair (ρ_1, ρ_2),

- how many eigenvalues are in the right half-plane, and
- how many eigenvalues are real/complex.

Here we give a direct way to construct a phase-diagram in the (ρ_1, ρ_2) plane which answers these questions.

The main approach that we take here is to exploit the low rank nature of the perturbations, along with some geometric constructions for the quantities of interest. We'd like to begin with some general dimension-counting arguments. The matrix[1] $\widetilde{\mathbf{M}}$ is assumed to be a real $N \times N$ matrix. Real non-symmetric matrices will generically have a real eigenvalue of multiplicity higher than one on a set of codimension one. In a two-parameter model such as we are considering here this codimension one set divides the parameter space into open sets having a constant number of real eigenvalues. As one crosses this set the number of real eigenvalues changes by (generically) two. This motivates the following definition:

Definition 1. *We define the bifurcation curve to be the locus of points $\mathcal{V} = (\rho_1, \rho_2)$ for which $\widetilde{\mathbf{M}}$ has a real eigenvalue of multiplicity two or higher.*

For matrix problems, of course, there exists an algebraic procedure for determining the values in the (ρ_1, ρ_2) plane where the matrix has multiple eigenvalues. One can simply compute the discriminant (in λ) of the characteristic polynomial of the matrix $\widetilde{\mathbf{M}}$,

$$\mathrm{disc}_\lambda(\det(\widetilde{\mathbf{M}} - \lambda \mathbf{I})) = P(\rho_1, \rho_2),$$

which gives a polynomial in the parameters (ρ_1, ρ_2). The variety defined by the zero set of this polynomial

$$\mathcal{V} = \{(\rho_1, \rho_2) | P(\rho_1, \rho_2) = 0\}$$

determines the bifurcation curve. Unfortunately, this computation isn't really practical to carry out analytically for real problems: for a large matrix, $P(\rho_1, \rho_2)$ will be a polynomial of large degree and the zero set will be difficult to compute. For the case of operators, even very nice ones, it is not clear that the discriminant makes sense at all. One might try to truncate to a matrix problem and construct the bifurcation curve for that finite dimensional system, but this approach seem unsatisfatory.

[1] For purposes of exposition we will consider the case where $\widetilde{\mathbf{M}}$ is a matrix, but everything we say will apply equally to the case where $\widetilde{\mathbf{M}}$ is an operator of compact resolvent.

Instead we present an alternative approach which uses the fact that the non-self-adjoint terms are of finite rank. The fact that the perturbing terms are of finite rank allow us to (generically) give an explicit rational or algebraic parameterization of the bifurcation curve. We begin by stating a preliminary lemma, which is basically the Aronszajn-Krein formula for rank one perturbations:

Lemma 1. *Let $\tilde{M}$ be an $N \times N$ matrix defined as in Equation (1). The characteristic polynomial of $\widetilde{\mathbf{M}}$*

$$\widetilde{D}(\lambda) = \det(\widetilde{\mathbf{M}} - \lambda \mathbf{I})$$

takes the following form:

$$\det(\widetilde{\mathbf{M}} - \lambda \mathbf{I}) = D(\lambda) + P_1(\lambda)\rho_1 + P_2(\lambda)\rho_2 + Q(\lambda)\rho_1\rho_2 \tag{2}$$

where $D(\lambda) = \det(\mathbf{M} - \lambda \mathbf{I})$ is the determinant of the unperturbed problem, $P_i(\lambda)$ are polynomials of degree (at most) $(N-1)$ and $Q(\lambda)$ of degree (at most) $N-2$. In the case where $\vec{f}_1$ and $\vec{f}_2$ (or $\vec{g}_{1,2}$) are linearly dependent $Q(\lambda) = 0$.

Proof. Due to the rank two nature of the perturbation, the characteristic polynomial can contain no powers of ρ_1 or ρ_2 above the first. The easiest way to see this is via multilinear algebra. The determinant is clearly polynomial in λ, ρ_1, ρ_2. A general term of the form $\rho_1^j \rho_2^k$ comes from the wedge product of j factors of $\vec{g}_1$, k factors of $\vec{g}_2$ and $(N-(j+k))$ columns from $\mathbf{M} - \lambda \mathbf{I}$. Any term with more than one factor of $\vec{g}_1$ and one factor of g_2 must be zero. Hence the determinant is of the above form.

The explicit form of the polynomials $P_i(\lambda), Q(\lambda)$ is easy to compute from the above construction. If we let $\mathrm{cof}^t(\mathbf{M} - \lambda \mathbf{I})$ denote the transpose cofactor matrix of $\mathbf{M} - \lambda \mathbf{I}$ then one has the following formulae

$$\begin{aligned}
P_1(\lambda) &= \langle \vec{f}_1, \mathrm{cof}^t(\mathbf{M} - \lambda \mathbf{I})\, \vec{g}_1 \rangle = \sum_i \langle \vec{f}_1, \phi_i \rangle \langle \vec{g}_1, \phi_i \rangle \prod_{j \neq i} (\lambda_j - \lambda) \\
P_2(\lambda) &= \langle \vec{f}_2, \mathrm{cof}^t(\mathbf{M} - \lambda \mathbf{I})\, \vec{g}_2 \rangle = \sum_i \langle \vec{f}_2, \phi_i \rangle \langle \vec{g}_2, \phi_i \rangle \prod_{j \neq i} (\lambda_j - \lambda) \\
Q(\lambda) &= \frac{1}{\det(\mathbf{M} - \lambda \mathbf{I})} \begin{vmatrix} \langle \vec{f}_1, \mathrm{cof}^t(\mathbf{M} - \lambda \mathbf{I})\, \vec{g}_1 \rangle & \langle \vec{f}_1, \mathrm{cof}^t(\mathbf{M} - \lambda \mathbf{I})\, \vec{g}_2 \rangle \\ \langle \vec{f}_2, \mathrm{cof}^t(\mathbf{M} - \lambda \mathbf{I})\, \vec{g}_1 \rangle & \langle \vec{f}_2, \mathrm{cof}^t(\mathbf{M} - \lambda \mathbf{I})\, \vec{g}_2 \rangle \end{vmatrix} \\
&= \sum_{i,j} \Big(\langle \vec{f}_1, \phi_i \rangle \langle \vec{g}_1, \phi_i \rangle \langle \vec{f}_2, \phi_j \rangle \langle \vec{g}_2, \phi_j \rangle - \langle \vec{f}_1, \phi_i \rangle \langle \vec{g}_2, \phi_i \rangle \langle \vec{f}_2, \phi_j \rangle \langle \vec{g}_1, \phi_j \rangle \Big) \prod_{k \neq i,j} (\lambda_k - \lambda)
\end{aligned}$$

where λ_i, ϕ_i are the eigenvalues and eigenvectors of the unperturbed matrix $\mathbf{M}$. □

It is often more convenient to divide (2) by $\det(\mathbf{M} - \lambda \mathbf{I})$ to put the eigenvalue condition in the form

$$1 = \rho_1 \langle f_1, (\mathbf{M} - \lambda \mathbf{I})^{-1} g_1 \rangle + \rho_2 \langle f_1, (\mathbf{M} - \lambda \mathbf{I})^{-1} g_1 \rangle.$$

This form has the advantage that it is expressed in terms of resolvents (i.e. $\mathbb{R}(\lambda) \equiv (\mathbf{M} - \lambda \mathbf{I})^{-1}$), which are defined very generally for operators, rather than determinants and cofactors, which are typically not well-defined for operators.

One geometric way to interpret this characteristic polynomial is as defining a one parameter family of rational curves, the curves of constant eigenvalue. For each value of λ one finds a curve in the (ρ_1, ρ_2) plane

along which λ is an eigenvalue. For instance the matrix has zero as an eigenvalue along the curve

$$D(0) + \rho_1 P_1(0) + \rho_2 P_2(0) + \rho_1\rho_2 Q(0) = 0$$
$$\rho_2 = -\frac{D(0) + \rho_1 P_1(0)}{P_2(0) + \rho_1 Q(0)}$$

in the (ρ_1, ρ_2) plane. In the special case where $Q(x) \equiv 0$ this defines a one-parameter family of lines. Given a family of curves it is always fruitful to consider the envelope of the family of curves, the simultaneous solution to

$$D(\lambda) + \rho_1 P_1(\lambda) + \rho_2 P_2(\lambda) + \rho_1\rho_2 Q(\lambda) = 0 \tag{3}$$
$$D'(\lambda) + \rho_1 P_1'(\lambda) + \rho_2 P_2'(\lambda) + \rho_1\rho_2 Q'(\lambda) = 0 \tag{4}$$

Whereas each curve in the family encodes information on the location of a particular eigenvalue the envelope of the curve encodes information on eigenvalue coincidence. This is the content of the next lemma. To simplify notation, we use the wedge notation for Wronskians: $f \wedge g = fg' - f'g$.

Lemma 2. *The solutions to (3, 4) give the bifurcation curve $\mathcal{V}$. If $Q(x)$ is not identically zero the bifurcation curve $\mathcal{V}$ is generically given by the union of the pair of parametric curves given by*

$$\rho_1 = \frac{-(P_1 \wedge P_2 + D \wedge Q) \pm \sqrt{(P_1 \wedge P_2 - D \ \wedge Q)^2 - 4(D \wedge P_1)(P_2 \wedge Q)}}{P_1 \wedge Q} \tag{5}$$

$$\rho_2 = \frac{P_1 \wedge P_2 - D \wedge Q \mp \sqrt{(P_1 \wedge P_2 - D \wedge Q)^2 - 4(D \wedge P_1)(P_2 \wedge Q)}}{P_2 \wedge Q}. \tag{6}$$

If $Q(x)$ is identically zero then the bifurcation curve is generically given by the parametric curve

$$\rho_1 = -\frac{P_2 \wedge D(\lambda)}{P_1 \wedge P_2(\lambda)} \tag{7}$$

$$\rho_2 = \frac{P_1 \wedge D(\lambda)}{P_1 \wedge P_2(\lambda)} \tag{8}$$

Proof. The equivalence of the envelope and the discriminant is standard - see for instance Bruce and Giblin[10] or Spivak[11]. Generically one just has to solve equations (3, 4) for ρ_1, ρ_2. This is equivalent to solving a linear and a quadratic equation in the general case and a pair of linear equations in the special case $Q(x) = 0$.

The problem in solving for $\rho_{1,2}$ is that it may happen that for some values of λ that the system (4) may be underdetermined and consistent and have an infinite number of solutions. For instance, in the special case $Q(x) = 0$, this occurs exactly when the matrix

$$\begin{pmatrix} D(\lambda) & P_1(\lambda) & P_2(\lambda) \\ D'(\lambda) & P_1'(\lambda) & P_2'(\lambda) \end{pmatrix}$$

fails to have full rank. In the general case the bifurcation curve is equal to the envelope curve as long as

none of the following conditions **C1**, **C2**, **C3** hold for any real λ :

$$\textbf{C1} \qquad \operatorname{rank}\begin{pmatrix} D & P_1 & P_2 & Q \\ D' & P_1' & P_2' & Q' \end{pmatrix} < 2 \tag{9}$$

$$\textbf{C2} \qquad \begin{cases} P_1 \wedge Q(\lambda) \neq 0 \\ P_2 \wedge Q(\lambda) = 0 \\ D \wedge P_1(\lambda) = 0 \\ P_1 \wedge P_2(\lambda) = D \wedge Q(\lambda) \end{cases} \tag{10}$$

$$\textbf{C3} \qquad \begin{cases} P_2 \wedge Q(\lambda) \neq 0 \\ P_1 \wedge Q(\lambda) = 0 \\ D \wedge P_2(\lambda) = 0 \\ P_2 \wedge P_1(\lambda) = D \wedge Q(\lambda) \end{cases} \tag{11}$$

If these genericity conditions fail for some value of λ then (generically) there exists a curve in the (ρ_1, ρ_2) plane along which that value of λ is a multiple eigenvalue. Note that one can always check whether or not a pair of polynomials have a common root by computing the resultant of the polynomials: one need *not* be able to explicitly factor the polynomials to test this condition. Thus the genericity condition is readily checkable. □

Lemma 3. *As (ρ_1, ρ_2) are varied so as to cross the envelope the number of real eigenvalues generically changes by two.*

Sketch. First we consider the case where $Q(\lambda)$ is identically zero, and the constant eigenvalue curves are lines. In a neighborhood of any point on the envelope curve with non-vanishing curvature the envelope divides the plane into two regions: one which is multiply (typically doubly) covered by lines of constant eigenvalue, and one which is not covered by any lines of constant eigenvalue; the latter is the side which contains the center of curvature. In the region that is doubly covered by the lines of constant eigenvalue a given point is on two lines, and thus has two distinct real eigenvalues. As this point approaches the envelope the eigenvalues approach each other, and as the point passes through the envelope there are no longer any lines of constant eigenvalue passing through the point, and thus no nearby real eigenvalues. Since the eigenvalues must vary continuously with the parameters, this implies that there must be a nearby complex conjugate pair. Thus the envelope of the family of constant eigenvalue lines also represents a bifurcation curve where a pair of real eigenvalues bifurcates to a complex conjugate pair.

It is possible that in a degenerate situation there is a component of the envelope consisting of an isolated point. In this case there is no bifurcation. This is, however, non-generic: under perturbation this point will either disappear or open to a small closed curve (across which there will be a bifurcation). Similarly it is possible that a portion of the envelope curve is swept out k times. In this case the number of real eigenvalues will change by $2k$ as the bifurcation curve is crossed. Again this situation will not persist under a generic perturbation, which will break the k-fold covered portion into k distinct curves.

For non-zero $Q(\lambda)$ the picture is similar, except that the curves of constant eigenvalue are rational functions and not lines. The general picture is illustrated in Figure (1), which shows a close-up of the envelope curve from an example to follow. On one side of the envelope curve there are two constant eigenvalue

curves (in light solid) that intersect each other. This intersection indicates that there are two nearby real eigenvalues, one corresponding to each constant eigenvalue curve. As the point of intersection moves toward the envelope curve (bold solid) the eigenvalues approach each other. At the envelope the eigenvalues coincide and the constant eigenvalue curve and envelope are tangent. On the other side of the envelope there are no (nearby) constant eigenvalue curves through a given point, hence the real eigenvalue pair has bifurcated to a complex conjugate pair. The main difference from the previous case is that the condition for determining the direction of the bifurcation is more complicated (than determining the direction of curvature), and involves the curvatures of the envelope and the constant eigenvalue curves themselves. □

Figure 1 here

We would next like to consider the possibility of eigenvalues of higher multiplicity. The envelope curve is, in general, a well behaved curve and admits a parametrization by arc-length. However this may fail at an isolated set of points in (ρ_1, ρ_2). The next lemma say that (modulo some genericity assumptions) the following are all equivalent, and occur on a codimension two set (isolated points in the (ρ_1, ρ_2) plane):

- Points in the (ρ_1, ρ_2) plane where the model has a real eigenvalue of multiplicity at least three.
- Points where the tangent vector to the envelope curve vanishes.
- Cusps in the envelope curve.

Lemma 4. *The vanishing of the tangent vector to the envelope curve at a point implies that the problem has an eigenvalue of multiplicity (at least) three at that point. The converse holds as long as the following determinant is non-zero at the point in question:*

$$\begin{vmatrix} P_1 + \rho_2 Q & P_2 + \rho_1 Q \\ P_1' + \rho_2 Q' & P_2' + \rho_1 Q' \end{vmatrix} \neq 0.$$

Alternatively, the model has a triple eigenvalue if and only if either

$$(P_1 \wedge P_2 \wedge Q)(P_1 \wedge P_2 \wedge D) = (D \wedge P_2 \wedge Q)(P_1 \wedge D \wedge Q) = 0$$
$$P_1 \wedge P_2 \wedge Q \neq 0$$

or

$$P_1 \wedge P_2 \wedge Q = P_1 \wedge P_2 \wedge D = D \wedge P_2 \wedge Q = P_1 \wedge D \wedge Q = 0.$$

Proof. The conditions for an eigenvalue of multiplicity (at least) two are given by (3,4). Differentiating each of these with respect to λ gives the following equations for ρ_1', ρ_2':

$$\rho_1'(P_1(\lambda) + \rho_2 Q(\lambda)) + \rho_2'(P_2(\lambda) + \rho_1 Q(\lambda)) = 0$$
$$\rho_1'(P_1'(\lambda) + \rho_2 Q'(\lambda)) + \rho_2'(P_2'(\lambda) + \rho_1 Q'(\lambda)) = -(D''(\lambda) + \rho_1 P_1''(\lambda) + \rho_2 P_2''(\lambda) + \rho_1\rho_2 Q'')$$

The conditions for an eigenvalue of multiplicity at least three are given by (3,4) together with the condition

$$(D''(\lambda) + \rho_1 P_1''(\lambda) + \rho_2 P_2''(\lambda) + \rho_1\rho_2 Q'') = 0. \tag{12}$$

Thus it is clear that $\rho_1' = 0, \rho_2' = 0$ implies that the eigenvalue is of multiplicity (at least) three. Further if

$$\begin{vmatrix} P_1 + \rho_2 Q & P_2 + \rho_1 Q \\ P_1' + \rho_2 Q' & P_2' + \rho_1 Q' \end{vmatrix} \neq 0$$

then the above system can be solved uniquely for ρ_1', ρ_2' and the existence of an eigenvalue of multiplicity three implies $\rho_1' = 0, \rho_2' = 0$.

A bit more algebra gives another characterization of points where the eigenvalue has multiplicity three or higher. Equations (3,4,12) form a system of three equations in three unknowns ρ_1, ρ_2, and $\rho_3 = \rho_1\rho_2$.

Solving these three equations for (ρ_1, ρ_2, ρ_3) and imposing the consistency condition $\rho_3 = \rho_1\rho_2$ shows that one has a root of multiplicity three if and only if either

$$(P_1 \wedge P_2 \wedge Q)\,(P_1 \wedge P_2 \wedge D) = (D \wedge P_2 \wedge Q)\,(P_1 \wedge D \wedge Q)$$
$$P_1 \wedge P_2 \wedge Q \neq 0$$

or all of the Wronskians

$$P_1 \wedge P_2 \wedge Q = P_1 \wedge P_2 \wedge D = D \wedge P_2 \wedge Q = P_1 \wedge D \wedge Q = 0$$

vanish. The first possibility is typically of codimension two - it is expected to occur at isolated values of λ corresponding to isolated values of (ρ_2, ρ_1). The second does not typically happen at all, since it requires the simultaneous vanishing of several polynomials. However in Example (1) this case occurs because it is forced by a symmetry of the model.

Finally recall that a simple zero of the tangent vector represents a cusp, and generically an eigenvalue of multiplicity at least three will have multiplicity exactly three, so typically cusps in the envelope are equivalent to triple eigenvalues. □

The geometry of a bifurcation in the neighborhood of a triple eigenvalue is illustrated in Figure 4B. In a neighborhood of this point there are three dominant eigenvalues which participate in the bifurcation. The cusp of the envelope represents a transition between a bifurcation between the intermediate and the smallest eigenvalue in the trio, and a bifurcation between the intermediate and the largest eigenvalue in the trio. Emerging from the cusp-point is a curve that represents an exchange of dominance phenomenon, with a complex conjugate pair of eigenvalues crossing a single real one.

When considering questions of stability and the behavior of the dominant eigenvalue it is also important to understand the behavior of the complex eigenvalues. In particular one would like to understand the locus of points at which the matrix has purely imaginary eigenvalues, as this curve indicates where the model loses stability due to a Hopf bifurcation.

Definition 2. *The Hopf curve is the locus of points in the (ρ_2, ρ_1) plane where $M(\rho_2, \rho_1)$ has a pair of purely imaginary eigenvalues. Generically this curve is given parametrically by*

$$\mathrm{Re}(D(i\omega)) + \rho_1 \mathrm{Re}(P_1(i\omega)) + \rho_2 \mathrm{Re}(P_2(i\omega)) + \rho_1\rho_2 \mathrm{Re}(Q(i\omega)) = 0 \tag{13}$$
$$\mathrm{Im}(D(i\omega)) + \rho_1 \mathrm{Im}(P_1(i\omega)) + \rho_2 \mathrm{Im}(P_2(i\omega)) + \rho_1\rho_2 \mathrm{Im}(Q(i\omega)) = 0, \tag{14}$$

where Re, Im *represent the real and imaginary parts respectively. The genericity conditions are the same as in Lemma (2) with the replacement of the Wronskians* $f \wedge g$ *by the quantities* $\mathrm{Re}(f(i\omega))\mathrm{Im}(g(i\omega)) - \mathrm{Re}(g(i\omega))\mathrm{Im}(f(i\omega))$.

The Hopf curve, the envelope, and the $\lambda = 0$ eigenvalue curve will all intersect at a single point, the point at which there is a zero eigenvalue of higher multiplicity. We now present an illustrative example.

Example 1. *We consider the following model:*

$$\mathbf{M} = \begin{pmatrix} -2 & -1 & 0 & -\rho_1 \\ -1 & -2 & -\rho_2 & 0 \\ \sqrt{2} & 1 & -2 & 0 \\ 1 & \sqrt{2} & 0 & -2 \end{pmatrix}.$$

It is straightforward to compute that the characteristic polynomial of this matrix is given by

$$\begin{aligned} \det(\mathbf{M} - \lambda \mathbf{I}) = (1+\lambda)(2+\lambda)^2(3+\lambda) + \left(\lambda^2 + (4-\sqrt{2})\lambda + (4-2\sqrt{2})\right)\rho_1 \\ + \left(\lambda^2 + (4-\sqrt{2})\lambda + (4-2\sqrt{2})\right)\rho_2 - \rho_1\rho_2 \end{aligned}$$

The zero eigenvalue curve is given by

$$\begin{aligned} 12 + (4-2\sqrt{2})\rho_1 + (4-2\sqrt{2})\rho_2 - \rho_1\rho_2 = 0 \\ \rho_1 = \frac{12 + (4-2\sqrt{2})\rho_2}{\rho_2 - (4-2\sqrt{2})} \end{aligned}$$

The bifurcation curve is given by the envelope

$$\begin{aligned} \rho_1 = -(\lambda+2)\left(\lambda + 2 + \frac{\sqrt{2}}{2}\right) \pm (\lambda+2)\sqrt{2\left(\lambda+\frac{3}{2}\right)\left(\lambda+\frac{5}{2}\right)} \\ \rho_2 = -(\lambda+2)\left(\lambda + 2 + \frac{\sqrt{2}}{2}\right) \mp (\lambda+2)\sqrt{2\left(\lambda+\frac{3}{2}\right)\left(\lambda+\frac{5}{2}\right)} \end{aligned}$$

together with the singular piece $\rho_1 = -\frac{1}{2} \cup \rho_2 = -\frac{1}{2}$*, which is associated to the value* $\lambda = -2 + \frac{\sqrt{2}}{2}$*, where the equations defining the envelope fail to have full rank. The envelope and the singular piece of the bifurcation curve meet tangentially at* $(\rho_2 = -\frac{1}{2}, \rho_1 = -\frac{3}{2})$ *and* $(\rho_2 = -\frac{1}{2}, \rho_1 = -\frac{3}{2})$*. Because of the symmetry we have* $P_1 = P_2$ *and thus* $P_1 \wedge P_2 \wedge Q \equiv 0$*, so the condition for a triple eigenvalue reduces to simultaneous vanishing of* $P_1 \wedge D \wedge Q$ *and* $D \wedge P_2 \wedge Q$*. Note that since* $P_1 = P_2$ *these are not independent —* $P_1 \wedge D \wedge Q = -D \wedge P_2 \wedge Q$*. Calculating we find that the triple eigenvalue condition becomes*

$$P_1 \wedge D \wedge Q = -16\lambda^3 + (12\sqrt{2} - 96)\lambda^2 + (48\sqrt{2} - 192)\lambda + (46\sqrt{2} - 128) = 0$$

This cubic has three real roots: a double root at $\lambda = -2 + \frac{\sqrt{2}}{2}$ *and a simple root at* $\lambda = -(\frac{1}{2} + \frac{\sqrt{2}}{4}) \approx -2.35$*. Recall that the envelope is not defined for* $\lambda \in (-\frac{5}{2}, -\frac{3}{2})$*, so the root at* $\lambda = -(\frac{1}{2} + \frac{\sqrt{2}}{4})$ *does not correspond to a real multiple eigenvalue. Thus the only real eigenvalue of multiplicity higher than two is* $\lambda = -2 + \frac{\sqrt{2}}{2}$.

Since this eigenvalue is associated to the singular piece of the bifurcation curve we can potentially have many points where this is a triple eigenvalue. Along the curve $\rho_1 = -\frac{1}{2}$ *the eigenvalues are*

$$\lambda = -2 + \frac{\sqrt{2}}{2}, -2 + \frac{\sqrt{2}}{2}, -2 - \frac{\sqrt{2}}{2} \pm \frac{\sqrt{2 - 4\rho_2}}{2}.$$

So the only triple eigenvalue is at $\rho_2 = -\frac{3}{2}$*, the point of intersection with the envelope curve. A similar calculation holds along* $\rho_2 = -\frac{1}{2}$*.*

The Hopf curve is given parametrically by

$$\rho_1 = (4 + \sqrt{2}) \frac{(4\omega^2 - 14) \pm \sqrt{30(18 - 8\sqrt{2} + (1 - 2\sqrt{2})\omega^2 + \omega^4)}}{14} \tag{15}$$

$$\rho_2 = (4 + \sqrt{2}) \frac{(4\omega^2 - 14) \mp \sqrt{30(18 - 8\sqrt{2} + (1 - 2\sqrt{2})\omega^2 + \omega^4)}}{14}, \tag{16}$$

where, as always, the signs are not *independent. Note that the argument of the square root is strictly positive, so there exists purely imaginary eigenvalues corresponding to oscillations of any desired frequency. The Hopf curve, the envelope, and the zero eigenvalue line all meet at the points* $(\rho_1 = (4 + \sqrt{2})(-1 \pm \frac{\sqrt{30(18 - 8\sqrt{2})}}{14}) = 4 + \sqrt{2} \pm \sqrt{30}, \rho_2 = (4 + \sqrt{2})(-1 \mp \frac{\sqrt{30(18 - 8\sqrt{2})}}{14}) = -(4 + \sqrt{2}) \mp \sqrt{30}$*. The most interesting region of the stability diagram is depicted in Figure (2). The zero eigenvalue curve is depicted in dashed red, the envelope in blue (including a dot at the origin), the singular piece of the bifurcation curve in dot-dashed magenta, and the Hopf curve in solid dotted green.*

From this information it is easy to derive the stability diagram. At the origin the eigenvalues are $\lambda = -3, \lambda = -2, \lambda = -2, \lambda = -1$*. Since there is a degenerate eigenvalue one needs to do a local perturbation analysis near* $\lambda = -2, \rho_1 = 0, \rho_2 = 0$ *to determine if in the neighborhood of this point one has a real pair of eigenvalues or a complex conjugate pair. Letting* $\lambda = -2 + \delta$ *shows that near this point one has*

$$\det(\mathbf{M} - \lambda \mathbf{I}) = -\delta^2 - \sqrt{2}\delta\rho_1 - \delta\sqrt{2}\rho_2 - \rho_1\rho_2 + O(3),$$

where $O(3)$ *denotes terms of order three or higher in* δ, ρ_i*. The discriminant of the above is* $(\sqrt{2}\rho_1 + \sqrt{2}\rho_2)^2 - 4\rho_1\rho_2 = 2\rho_1^2 + 2\rho_2^2 > 0$*, indicating that in a neighborhood of the origin the double eigenvalue splits into a real (distinct) pair of eigenvalues. Thus in the region containing the origin and bounded by the singular pieces of the bifurcation curve and the upper branch of the envelope (labelled* $\mathbf{A}$*) there are four real eigenvalues in the left half-plane. As* ρ_2 *is decreased so as to cross the line* $\rho_2 = -\frac{1}{2}$ *the first bifurcation occurs. Since this line corresponds to eigenvalue* $\lambda = -2 + \sqrt{2}$ *and* $-2 < -2 + \frac{\sqrt{2}}{2} < -1$ *the bifurcation consists of the two dominant real eigenvalues bifurcating to a complex conjugate pair. Thus in region* $\mathbf{B}$ *we have two real eigenvalues and two complex eigenvalues, all in the left half-plane. As one leaves region* $\mathbf{B}$ *across the Hopf curve into the region labelled* $\mathbf{E}$ *the complex conjugate pair moves into the right half-plane, giving two complex eigenvalues in the right half-plane and two real eigenvalues in the left half-plane. Proceeding in this fashion the stability diagram can be labelled as follows:*

- *Region A: Four real eigenvalues in the left half-plane.*
- *Region B: Two real and two complex eigenvalues in the left half-plane.*
- *Region C: Four complex eigenvalues in the left half-plane.*

- *Region D: Two complex eigenvalues in right half-plane, two complex eigenvalues in the left half-plane.*
- *Region E: Two complex eigenvalues in the right half-plane, two real eigenvalues in the left half-plane.*
- *Region F: One real eigenvalue in the right half-plane, three real eigenvalues in the left half-plane.*
- *Region G: One real eigenvalue in the right half-plane, one real and two complex eigenvalues in the left half-plane.*

Additionally there is a narrow region between the regions labelled **E** and **F** (to the left of $\rho_2 = -(4 + \sqrt{2}) - \sqrt{30} \approx -10.9$ above the zero eigenvalue curve and below the envelope curve) where there are two real eigenvalues in the left half-plane and two real eigenvalues in the right half-plane. This region is not labelled since it is not visible on this scale.

One feature which we have not labelled are points where a real eigenvalue and a complex conjugate pair all have the same real part, corresponding to points where a real eigenvalue and a complex conjugate pair exchange dominance. Although it is easy to write down an implicit equation satisfied by these curves, it is generally not possible to find an explicit formula as for the Hopf curve, envelope, etc.

Since the characteristic polynomial of this problem is of order four it would in principle be possible to extract the above information directly from the solution formula for the quartic. In practice it would be exceedingly difficult to recover such detailed information. In the next section we will consider a model of the oculomotor neural integrator given by a differential equation of order eight; in this situation it is no longer possible even in principle to state a direct formula for the roots.

Figure 2 here

In this section, we established a procedure for computing constant eigenvalue curves, bifurcation curves, and cusps of low-rank perturbations of self-adjoint operators. We now apply this procedure to three applications, which can be written in the form of Eqn. (1). The first is a model of a coupled brainstem-cerebellum neuronal network called the *oculomotor integrator* (§2); the second is a continuum version of that model, in which the (relatively numerous) brainstem neurons are replaced by a continuum (§3). Finally, we analyze a stability problem that arises in a nonlocal reaction-diffusion equation [2] (§4).

2 Example: a model for the oculomotor integrator

The *oculomotor integrator* is an neural network that contributes an essential position command to eye movement control. It receives eye velocity commands from oculomotor subsystems such as the vestibular and saccadic systems and transforms them to position commands through temporal integration [12, 13]. We will present a model for the oculomotor integrator which can either simulate normal integrator function, or a common eye movement disorder — congenital or *infantile nystagmus* (IN) — with a few small changes. We are able to make this determination by analysis of the envelope, constant eigenvalue curves and Hopf curve as in §1. Some of this analysis was presented in [14], which focused on using the model to simulate various eye movements associated with IN; here, we focus on analyzing the full phase space generated by the low-rank perturbations.

We first summarize the biological operation of the integrator, which form the basis for the model. The neurons that compose the integrator are located mainly in a brainstem region known as the *vestibular nucleus*. These neurons must integrate *velocity* signals into a desired *position*; thus, they perform the operation of integration. Single neurons produce a small amount of temporal integration in that their firing rates increase due to a transient input will decay with a time constant of about 5 ms. The overall oculomotor integrator network has a time constant closer to 20 s, so the integrator network must lengthen the single-neuron time constant by about 4000 times [13]. For a linear system, this corresponds to tuning an eigenvalue near zero. Furthermore, the integrator should have the right *gain* in response to velocity signals; the ratio of its response to the input should be appropriate. Ideally, it should also be *plastic*; it should be able to adjust, if injury or some other change occurs (for example, you adjust your oculomotor integrator gain this every time you get a new pair of glasses) [15, 16, 17, 18].

What is the network structure that underlies this function? One hypothesis for how the oculomotor integrator does this is through bilateral inhibition [19]. Proper function, including generation of a full-length, 20 s integrator time constant and control of integrator gain, requires connections between the vestibular nuclei and the cerebellum[20, 21, 22]: lesion studies show that these connections are needed both for normal operation and for plasticity [23, 24, 25, 26].

Critically, neuroanatomical findings reveal two essential asymmetries in the vestibular-cerebellar interaction. First, while there are numerous connections from the vestibular nucleus to the cerebellum, the feedback connections from the cerebellum are relatively sparse and are inhibitory [27, 28, 29, 30, 31, 32]. Second, while the vestibular nuclei and the cerebellum, like the rest of the brain, are bilateral structures, the vestibular nuclei on both sides project to the cerebellum on both sides, but the cerebellum projects back to the vestibular nuclei on the same side only. Anastasio and Gad [1] showed previously that this asymmetry permits the cerebellum to sensitively control the both the time constant and the gain of the oculomotor integrator, despite (or perhaps because) the projections from the cerebellum back to the vestibular nuclei are so sparse. These sparse cerebellar-to-vestibular connections, which can plastically change their strength, are precisely the low-rank perturbations we analyze in detail here.

Anastasio and Gad [1] proposed a linear differential equation model that combined a bilateral inhibitory vestibular network with sparse, asymmetric feedback connections from cerebellar *Purkinje cells*, i.e., the evolution of the system is given by:

$$\frac{d\vec{v}}{dt} = \mathbf{M}\vec{v} + s(t)\vec{b} \qquad \vec{v}(0) = \vec{0}, \tag{17}$$

where $\vec{v}$ represents the response of the system (vestibular neurons and Purkinje cells together), $\mathbf{M}$ represents a matrix of connections, $s(t)$ is a scalar input (velocity) signal to the integrator, and $\vec{b}$ a fixed vector representing the pattern in which the vestibular neurons receive the input signal.

The connection matrix $\mathbf{M}$ proposed is:

$$\mathbf{M} = \alpha \begin{pmatrix} \mathbf{T} & -\rho_1\vec{u}_1 & -\rho_2\vec{u}_2 \\ \vec{w}_1^t & -1 & 0 \\ \vec{w}_2^t & 0 & -1 \end{pmatrix} \tag{18}$$

The vestibular neuron-to-Purkinje cell coupling vectors are given by the $\vec{w}_i$; the Purkinje cell-to vestibular

neuron coupling vectors are given by $(\vec{u}_1)_j = \delta_{j,k_1}, (\vec{u}_2)_j = \delta_{j,k_2}$. The matrix $\mathbf{T}$ of effective connections between vestibular neurons is given by

$$\mathbf{T} = \begin{pmatrix} -1+\beta & \beta & 0 & 0 & \cdots & 0 \\ \beta & -1+\beta & \beta & 0 & \cdots & 0 \\ \vdots & \vdots & \vdots & \vdots & \ddots & \vdots \\ 0 & 0 & 0 & 0 & \beta & -1+\beta \end{pmatrix}. \tag{19}$$

The parameter α is set to $200\,\mathrm{s}^{-1}$ (corresponding to a typical 5 ms membrane time constant); the parameter β is fixed so that the vestibular sub-network has a time constant of 0.2 s in the absence of cerebellar interaction ($\rho_1 = \rho_2 = 0$). The largest eigenvalue of $\mathbf{T}$ is given by $\lambda_1/\alpha = -1+\beta(1+2\cos(\frac{\pi}{N+1}))$, where N is the number of vestibular cells (on each side of the network); therefore we choose $\beta = \frac{\lambda_1/\alpha+1}{1+2\cos\left(\frac{\pi}{N+1}\right)}$, where $\lambda_1 = 5\,\mathrm{s}^{-1}$. We take the output of the integrator to be a linear readout of the vestibular neuron responses, which for simplicity we take to be equal to $\vec{b}$: i.e. $\langle \vec{b}, \vec{v}(t) \rangle$. Defining the eigenvectors $\vec{e}_i$ and adjoint eigenvectors $\vec{f}_i$ respectively by

$$\begin{aligned} \mathbf{M}\vec{e}_i &= \lambda_i \vec{e}_i \\ \mathbf{M}^t \vec{f} &= \lambda_i \vec{f}_i \end{aligned}$$

the linear readout at time t (assuming $\mathbf{M}$ diagonalizable) is given by

$$\langle \vec{b}, \vec{v}(t) \rangle = \sum_i \frac{\langle \vec{b}, \vec{e}_i \rangle \langle \vec{f}_i, \vec{b} \rangle}{\langle \vec{f}_i, \vec{e}_i \rangle} \int_0^t e^{\lambda_i (t-t')} s(t') dt'.$$

When there is a separation of time scales ($\mathrm{Re}(\lambda_2) \ll \mathrm{Re}(\lambda_1)$), the response is largely due to the dominant eigenvalue; we define the *gain*, γ, to be the ratio of this response, to the magnitude of the filtered input:

$$\begin{aligned} \langle \vec{b}, \vec{v}(t) \rangle &\approx \frac{\langle \vec{b}, \vec{e}_1 \rangle \langle \vec{f}_1, \vec{b} \rangle}{\langle \vec{f}_1, \vec{e}_1 \rangle} \int_0^t e^{\lambda_1 (t-t')} s(t') dt' && (20) \\ &= \frac{\langle \vec{b}, \vec{e}_1 \rangle \langle \vec{f}_1, \rangle}{\langle \vec{f}_1, \vec{e}_1 \rangle \|\vec{b}\|^2} \times \left[\|\vec{b}\|^2 \int_0^t e^{\lambda_1 (t-t')} s(t') dt' \right] && (21) \\ &= \gamma \left[\|\vec{b}\|^2 \int_0^t e^{\lambda_1 (t-t')} s(t') dt' \right] && (22) \end{aligned}$$

Thus, γ captures how the circuit amplifies — or suppresses — the incoming signal.

Setting this ratio correctly allows the organism to respond appropriately to its environment. However, injury or normal growth can alter the sensory systems that supply inputs to the integrator, and thus create a mismatch between input and desired output. To counteract this, the system must change this gain to compensate. We will allow our network to change, by adjusting the Purkinje-to-vestibular weights ρ_1 and ρ_2; this is biologically plausible, since one of the major functions of the cerebellum is to regulate motor plasticity and learning.

The asymmetry of the matrix $\mathbf{M}$ is crucial, to allow gain to be adjusted freely; for a symmetric (more generally *normal*) matrix, $-1 \leq \gamma \leq 1$. When can we get big changes in gain, with relatively small changes in

ρ_1 and ρ_2? It would be ideal for the denominator of γ to be near zero (assuming both $\vec{f}_1$, $\vec{e}_1$ are normalized to unit length): $\langle \vec{f}_1, \vec{e}_1 \rangle \ll 1$. However, this corresponds to near-orthogonality of the right and left eigenvectors, which occurs near a double eigenvalue (perfect orthogonality, $\langle \vec{f}_1, \vec{e}_1 \rangle = 0$, can occur only when there is a degenerate double eigenvalue).

We now show an example of an integrator that can perform normal integration with arbitrary adjustment of gain: let $\mathbf{T}$ be 6×6 and choose

$$\begin{aligned} \vec{u}_1 &= \vec{\mathbf{e}}_1, \qquad \vec{u}_2 = \vec{\mathbf{e}}_3 \\ \vec{w}_1^t &= \begin{bmatrix} -1 & 1 & -1 & 0 & -1 & 0 \end{bmatrix} \\ \vec{w}_2^t &= \begin{bmatrix} 1 & -1 & 1 & 1 & 0 & 0 \end{bmatrix} \end{aligned} \tag{23}$$

where $\vec{\mathbf{e}}_j$ is the jth identity vector (in this case $\vec{\mathbf{e}}_j \in \mathbb{R}^6$).
Figure 3 here

With this choice, $\mathbf{M}$ is the reduced matrix of a model with 6 vestibular neurons and 2 Purkinje cells on each side of the bilaterally symmetric network. The only parameters that may vary are ρ_1 and ρ_2, the strengths of the Purkinje-to-vestibular connections. In order to fix a certain time constant, ρ_2 and ρ_1 should be constrained to lie on the appropriate constant eigenvalue curve. The biologically appropriate time constant is in the neighborhood of 20 s, so the appropriate eigenvalue is $\lambda = -\frac{1}{20}$. From the results of §1 we know that this holds along the curve

$$Q(-\frac{1}{20})\rho_1\rho_2 + P_2(-\frac{1}{20})\rho_2 + P_1(-\frac{1}{20})\rho_1 + D(-\frac{1}{20}) = 0$$

or (approximately)

$$\rho_1 = \frac{0.137 + 2.536\rho_2}{1 + .371\rho_2} \tag{24}$$

This constant eigenvalue curve is tangent to the envelope at the simultaneous solution of

$$\begin{aligned} 0.137 - \rho_1 + 2.536\rho_2 - 0.371\rho_1\rho_2 &= 0 \\ 0.577 - \rho_1 + 2.405\rho_2 - 0.473\rho_1\rho_2 &= 0. \end{aligned}$$

(Note: we have divided each equation through by a constant.) The biologically important root of the above pair of equations is the one in the first quadrant, $(\rho_2, \rho_1) = (1.22, 2.23)$: negative values of ρ would correspond to an excitatory Purkinje to vestibular connection, which is not known to occur.

The basic picture of integrator operation is as follows: let us suppose that ρ_2 is allowed to vary but that ρ_1 is given by Eqn. (24), so that $\lambda = -\frac{1}{20}$ is always an eigenvalue. As ρ_2 is increased from zero the dominant eigenvalue is fixed at $\lambda = -\frac{1}{20}$ and the (in this case real) subdominant eigenvalue increases. Because we are nearing the envelope curve (and thus a degenerate double eigenvalue $\lambda_2 = \lambda_1 = -\frac{1}{20}$), we expect the gain to increase. At $\rho_2 = 1.22$, where the constant eigenvalue curve is tangent to the envelope, there is a collision of eigenvalues and the dominant eigenvalue is degenerate. As ρ_2 is further increased the formerly subdominant eigenvalue is now dominant - it is real and larger than $-\frac{1}{20}$. Furthermore, we can compute the

gain associated to the dominant mode along the $\lambda = -\frac{1}{20}$ curve and find

$$\gamma = \frac{\langle \vec{f}, \vec{b}\rangle\langle \vec{b}, \vec{e}\rangle}{\|\vec{b}\|^2\langle \vec{f},\ \vec{e}\rangle} \approx \frac{0.05(\rho_2 + 1.43)(\rho_2 + 1.86)}{(1.22 - \rho_2)(1.65 + \rho_2)}$$

Note that, as expected, the denominator of the gain diverges at $\rho_2 = 1.22$, where the constant eigenvalue curve is tangent to the envelope and the $\lambda = -\frac{1}{20}$ eigenvalue is degenerate.

In Figure 3A we show the response of the network to an impulsive forcing of the form $f(t) = \delta(t)(1, 1, 1, 1, 1, 1, 0, 0)^t$ as ρ_2, ρ_1 are varied to increase gain. (Note that the impulsive forcing is equivalent to free decay with a corresponding initial condition). Three responses are shown, with ρ_2 set to 0.65,0.955, and 1.095 respectively. For each value of ρ_2, ρ_1 is set so that the network lies on the constant time constant curve $\tau = 20s$. The gains predicted based on a single dominant mode (γ in Eqn. (22)) are $2.52, 5.92$ and 12.88. The measured maximum impulse responses are $30.48, 70.38, 150.35$ respectively. To estimate γ from the impulse response, we divide by the number of vestibular cells (corresponding to $\|\vec{b}\|^2$, here 12), yielding $2.54, 5.87, 12.53$ respectively. So we see excellent agreement.

Figure 3B displays the interaction of the two dominant eigenvalues of the network in the vicinity of the current operating region. In order to increase gain, the network must climb up the $\lambda = -0.05$ curve in the vicinity of the double eigenvalue point. At the intersection of this curve with the envelope, the integrating eigenvalue exchanges dominance with another real eigenvalue, producing an unstable integrator. Note that the larger two gain cases straddle the point where the $\lambda = -\frac{1}{20}\mathrm{s}^{-1}$ curve crosses the envelope, indicating an eigenvalue bifurcation in a subdominant mode. In this case it is the mode(s) with the next largest real part. At about $\rho_2 \approx 1.02$ the subdominant complex conjugate pair collides at the real axis, and for ρ_2 above this value the first three most dominant eigenvalues are all real. As ρ_2 increases the subdominant eigenvalue increases until $\rho_2 \approx 1.22$ where there is an eigenvalue collision and exchange of dominance.

Figure 3B also uses letter labels to show the character of the dominant eigenvalue. Normal operation requires the network to remain in regions A or G. If the network is in error, it may wander into a region where the two eigenvalues are complex (F), or into the region where one or both eigenvalues are in the right half-plane (B,C, D or E). In neither case is normal operation possible.

Infantile nystagmus (IN) is a hereditary disorder characterized by involuntary, periodic eye movements. These movements (or waveforms) can be broadly classified into two forms, *jerk* and *pendular*. In jerk waveforms, the eye moves outward from the central position with increasing speed until interrupted by a sudden saccade; a pendular waveform resembles a sinusoidal oscillation. The presence of a jerk waveform suggests an unstable eigenvalue ($\lambda > 0$); as noted in many integrator models, the need to maintain an eigenvalue very near zero implies that an unstable eigenvalue is a natural consequence of imprecision.

In our model, the ability to modulate gain is enhanced near the bifurcation curve; this suggests that the network is *also* near a complex pair, which would generate the sinusoidal oscillations characteristic of pendular nystagmus. In [14], we showed that this model could indeed display several waveforms observed in IN. Here, we repeat one example, emphasizing how it relies on the techniques of §1.

We now consider the network specified in Eqn. (25). This is very similar to Eqn. (23); the only change is that the vestibular-to-Purkinje input from a handful of neurons has been altered. Here, as the cerebellum

attempts to increase gain by adjusting ρ_1 and ρ_2, it enters an oscillating regime.

$$\begin{array}{rclcrcl} \vec{u}_1 & = & \vec{\mathbf{e}}_1, & & \vec{u}_2 & = & \vec{\mathbf{e}}_3 \\ \vec{w}_1^t & = & \left[\begin{array}{cccccc} -1 & 1 & 0 & 0 & -1 & 0 \end{array} \right] & & & & \\ \vec{w}_2^t & = & \left[\begin{array}{cccccc} 1 & -1 & 0 & 0 & 1 & 0 \end{array} \right] & & & & \end{array} \tag{25}$$

Figure 4 here

We see the impulse response of the network in Figure 4A. As in Fig. 3A, ρ_2 and ρ_1 are varied so as to remain along the $\lambda = -\frac{1}{20}\mathrm{s}^{-1}$ curve. As ρ_2 (and the gain) increase, the network enters a regime where an oscillation is superimposed on normal integration. Figure 4B illustrates why this behavior occurs. As we follow the $\lambda = -\frac{1}{20}\mathrm{s}^{-1}$ curve from left to right through Region A, gain will increase. However, the eigenvalue curve has an intersection with the Hopf curve far to the left of its intersection with the envelope. At this point the integrating eigenvalue exchanges dominance with a pair of imaginary eigenvalues. Beyond this point, the response of the network contains both the normal integrating mode and a superimposed oscillation (Region F).

3 Example: a continuum model of the oculomotor integrator

We next consider a continuum model that can be derived from the model of Anastasio and Gad by replacing the (relatively numerous) vestibular neurons with a continuum vestibular "line" denoted by $\psi(x)$, while the relatively few Purkinje cells remain discrete.

Suppose the network has N vestibular cells on each side of the integrator, arranged in a row of length L. The bilateral vestibular-vestibular inhibition has nearest-neighbor structure; each row of $\mathbf{T}$ takes the form $\beta v_{j-1} + (-1+\beta)v_j + \beta v_{j+1}$ (Eqn. (19)). This will converge, in the continuum limit ($N \to \infty$), to a second derivative, because:

$$\left(\frac{L}{N}\right)^2 \psi_{xx} \quad = \quad \psi_{i+1} + \psi_{i-1} - 2\psi_i + o\left(\left(\frac{L}{N}\right)^3\right)$$

The sum over vestibular cells in the equation for the Purkinje cells (two final rows of Eqn. (18)) is replaced by an integral:

$$\sum_j (\vec{w}_1^t)_j v_j \to \frac{1}{L/N} \int_0^L \psi(x)\phi_1(x)dx$$

where $\psi(j\Delta x) = v_j$ and $\phi_1(j\Delta x) = (\vec{w}_1^t)_j$.

This leads to the following integro-differential eigenvalue problem on $L_2[0,L]\times\mathbb{R}^2$

$$\beta(\Delta x)^2\psi_{xx}+(-1+3\beta)\psi-\rho_1P_1\delta(x-x_1)-\rho_2P_2\delta(x-x_2)=\lambda\psi, \tag{26}$$
$$\psi(0)=0,\qquad \psi(L)=0$$
$$-P_1+\frac{1}{\Delta x}\int_0^L\psi(x)\phi_1(x)dx=\lambda P_1 \tag{27}$$
$$-P_2+\frac{1}{\Delta x}\int_0^L\psi(x)\phi_2(x)dx=\lambda P_2 \tag{28}$$

where we have replaced L/N with Δx. We have also scaled the entire problem by the common factor of α. The delta function coupling reflects the sparseness of the Purkinje-to-vestibular connections, with $x_{1,2}$ denoting the points on the vestibular line innervated by the Purkinje cells, and the functions $\phi_{1,2}(x)$ represent the density of vestibular to Purkinje connections. In the absence of more detailed connection data we take $\phi_{1,2}$ to be constant, although the model can be analyzed in the same manner for essentially arbitrary connection patterns $\phi_{1,2}(x)$. Similarly the Purkinje-to-vestibular connections $\delta(x-x_i)$ could also be replaced by a more general profile, and a similar analysis would be straightforward.

Eliminating P_1, P_2 from the equation algebraically, we have the single equation

$$\psi_{xx}+\frac{-1+3\beta}{\beta(\Delta x)^2}\psi+\frac{\rho_1\langle\psi,1\rangle}{\beta(\Delta x)^3(\lambda+1)}\delta(x-x_1)+\frac{\rho_2\langle\psi,1\rangle}{\beta(\Delta x)^3(\lambda+1)}\delta(x-x_2)=\frac{\lambda}{\beta(\Delta x)^2}\psi,\qquad \psi(0)=0=\psi(L) \tag{29}$$

This model can be solved in much the same way as the discrete model analyzed in §2. To illustrate we take $L=1$ and (as previously mentioned) the vestibular-to-Purkinje connections to be $\phi_1(x)=\phi_2(x)=1$. Note that when $\rho_1=0,\rho_2=0$, the vestibular neurons decouple from the Purkinje cells and the problem becomes lower triangular. In this case the eigenvectors ψ are given by trigonometric functions with the appropriate boundary conditions:

$$\psi_n(x)=\sin(n\pi x) \tag{30}$$

after which P_1, P_2 are obtained by using Eqns. (27,28):

$$P_1=\frac{N^2(1-\cos(n\pi))}{n\pi\left(3\beta-\beta\left(\frac{n\pi}{N}\right)^2\right)} \tag{31}$$
$$P_2=\frac{N^2(1-\cos(n\pi))}{n\pi\left(3\beta-\beta\left(\frac{n\pi}{N}\right)^2\right)}. \tag{32}$$

The corresponding eigenvalues are given by $\lambda_n=-1+3\beta-\beta\frac{n^2\pi^2}{N^2}$, together with $\lambda=-1$, an eigenvalue of multiplicity two corresponding to the Purkinje cells. Note that the even modes ($n=2k$) do not actually excite a Purkinje cell response ($P_1=P_2=0$), and thus the even modes are eigenfunctions of this problem for all values of ρ_1,ρ_2: these modes do not change under perturbation by the Purkinje cells. Thus we only need track the odd eigenvalues $n=2k+1$.

One can apply the techniques developed earlier in the paper to find the lines of constant eigenvalue. We will not reproduce the entire calculation, but merely note a few salient points. The first step is to act on

Equation (26) with the appropriate resolvent (inverse) operator (here, $R_\lambda = (\beta(\Delta x)^2\partial_{xx} + 3\beta - (1+\lambda))^{-1}$). The terms $R_\lambda\delta(x - x_i)$ are simply the Green's function for the operator $\beta(\Delta x)^2\partial_{xx} + 3\beta - (1+\lambda)$ acting on $L_2[0, L]$ with Dirichlet boundary conditions, which can be easily calculated – see (for example) the text of Keener[33]; we also supply some details in the Appendix.

The main conclusion, is that the perturbed problem will have piecewise trigonometric eigenfunctions of the form $\sin(\omega x)$, etc. (with appropriate continuity conditions; see Eqn. (61)), where

$$\omega^2 = \frac{-\lambda - 1 + 3\beta}{\beta(\Delta x)^2} \Rightarrow \lambda = -1 + 3\beta - \beta(\Delta x)^2\omega^2 \tag{33}$$

We now fix the remaining constants in the model: $x_1 = \frac{1}{3}$ and $x_2 = \frac{1}{2}$, and perform the calculation thus described. We find that the resulting envelope curves have asymptotes when ω is a multiple of 4π and 6π; this is a consequence of the location of the Purkinje cell innervation (i.e. x_1 and x_2).

One issue that becomes apparent, is that as the network becomes large we are unable to find an integrating eigenvalue using Eqn (33) in this way; observe that λ is bounded above by $\lambda = -1 + 3\beta - \beta(\Delta x)^2\omega^2 <= -1 + 3\beta \approx -\frac{1}{40} + \frac{39}{120}\left(\frac{\pi}{N+1}\right)^2$, which $\to -\frac{1}{40}$ as $N \to \infty$. However, the desired eigenvalue for a 20 s time constant (recall that we have scaled out the 5 ms single neuron time constant, $\alpha = 200$) is $\lambda = -0.05/200$, which is much closer to zero than $-1/40$; as N increases, the integrating eigenvalue will become out of reach. One way to view this observation is that as ratio of vestibular to cerebellar (Purkinje) cells increases, sparse cerebellar innervation becomes less able to alter the time constant of the vestibular network.

The alternative, is to consider piecewise exponential eigenfunctions; i.e.

$$\psi(x) = \begin{cases} A\sinh\omega x, & x < x_1 \\ B\sinh\omega x + C\cosh\omega x, & x_1 < x < x_2 \\ D\sinh(\omega(L-x)), & x > x_2 \end{cases}$$

where now

$$\omega^2 = \frac{\lambda + 1 - 3\beta}{\beta(\Delta x)^2} \Rightarrow \lambda = -1 + 3\beta + \beta(\Delta x)^2\omega^2 \tag{34}$$

Although such functions cannot match the boundary conditions of the *unperturbed* problem, the discontinuities in the perturbed problem bring them back into consideration. We can plot the corresponding bifurcation curve; it begins near $(\rho_2, \rho_1) \approx (-0.09, 0.09)$ (for $N = 12$) and increases without bound into the second quadrant. In Fig. 5, we plot the phase plane for several values of N; $N = 12$, 24, 50 and 100. In each panel, we show several pieces of the bifurcation curve in different colors: $(0, 4\pi)$ (purple), $(4\pi, 6\pi)$ (blue), $(6\pi, 8\pi)$ (cyan), $(8\pi, 12\pi)$ (green), and the curve for exponential eigenfunctions (yellow). We note that the structure is stable, for increasing N; however, the corresponding values of λ are "compressed" (see Eqn. (33)). This is to be expected; in the finite-dimensional problem, the eigenvalues cluster together as N increases; therefore we expect increasing density of constant eigenvalue curves as N increases. There is also a singular piece of the bifurcation curve, for the eigenvalue $\lambda = -1$; this intersects the origin and is illustrated in pink (dash-dotted).

We now return to the question that originally motivated our analysis in §2; can this network behave as an integrator; i.e. can it achieve the correct time constant and gain, by adjusting its Purkinje-to-vestibular

weights ρ_1, ρ_2? As N increases, it does appear that the integrating eigenvalue line $\lambda = -0.05/200$ has a piece in the first quadrant; the integrator could maintain a correct time constant by navigating along this line (although we must first verify that this is the *dominant* eigenvalue, which we have not yet done). Unfortunately, the bifurcation point for $\lambda = -0.05/200$ — indeed, for any eigenvalue near zero — is in the second quadrant, which is an unphysical location. Therefore, it is unlikely that this network — where $\phi_1 = \phi_2 = 1$, $x_{1,2} = \{1/3, 1/2\}$, and plasticity comes from manipulating the strength of the Purkinje-to-vestibular connections ρ_1, ρ_2 — can regulate both time constant *and* gain.

What is new here (from §2), is that the continuum model has given us a way to draw conclusions about a *family* of networks that is independent of system size N (as long as N is sufficiently large). We now take one further step in generality, by asking how the network behaves as the Purkinje-to-vestibular connection *locations* – x_1 and x_2 – change.

Recall that a necessary condition for the network to perform as an integrator, is for the $\lambda = -0.05/200$ bifurcation point to occur in the first quadrant (i.e. both $\rho_2, \rho_1 > 0$). We will show that for the vestibular-to-Purkinje projection patterns chosen here, the ρ_1, ρ_2 coordinates of the bifurcation point will always be of opposite sign, and therefore not physiologically plausible. We begin by observing that

$$D(\omega) = -1 \tag{35}$$

$$P_1(\omega) = \frac{-1 + \cosh(\omega x_1) - \sinh(\omega x_1)\tanh\left(\frac{\omega}{2}\right)}{\beta^2(\Delta x)^3\omega^2(3+\omega\Delta x)^2} \tag{36}$$

$$P_2(\omega) = \frac{-1 + \cosh(\omega x_2) - \sinh(\omega x_2)\tanh\left(\frac{\omega}{2}\right)}{\beta^2(\Delta x)^3\omega^2(3+\omega\Delta x)^2} \tag{37}$$

Note that

$$P_1(\omega) = f(\omega, x_1), \qquad P_2(\omega) = f(\omega, x_2)$$

for the same function $f(\omega, x)$. Then by Eqns. (7, 8) the coordinates of the bifurcation point will be:

$$\begin{aligned} \rho_1 &= -\frac{\partial P_2}{\partial \omega} \times \left(\frac{1}{P_1 \wedge P_2(\omega)}\right) \\ \rho_2 &= \frac{\partial P_1}{\partial \omega} \times \left(\frac{1}{P_1 \wedge P_2(\omega)}\right); \end{aligned}$$

consequently,

$$\frac{\rho_1}{\rho_2} = -\frac{\frac{\partial f}{\partial \omega}(\omega, x_2)}{\frac{\partial f}{\partial \omega}(\omega, x_1)}$$

We will argue that in fact, $\frac{\partial f}{\partial \omega}(\omega, x) > 0$ for $\omega > 0$ and $0 < x < 1$; therefore, the ratio of ρ_1 and ρ_2 must be negative.

For simplicity, we take $\lambda = 0$; then by Eqn. (34) the corresponding value of $\omega^2 = \frac{1-3\beta}{\beta(\Delta x)^2}$. Differentiating the function $f(\omega, x)$ given in Eqn. (37) and making this substitution, we find that

$$\begin{aligned} \frac{\partial f}{\partial \omega}(\omega, x) = &\frac{\operatorname{sech}^2\left(\frac{\omega}{2}\right)}{2(-1+3\beta)\omega\Delta x} \times \\ &\Big[(4-6\beta)\left(\cosh(\omega x) + \cosh(\omega(1-x)) - 1 - \cosh(\omega)\right) + \omega\left((1-x)\sinh(\omega x) + x\sinh(\omega(1-x))\right)\Big] \end{aligned} \tag{38}$$

(we have continued to use the symbol ω where it simplifies the presentation, although ω is now a function of β and Δx). The quantity $-1+3\beta$ is negative for $N > 10$; therefore it remains to show that the quantity in square brackets ($[\ldots]$) is negative as well.

First, we (re-)define the bracketed quatity

$$F_\omega(x) = \Big[(2+a)\left(\cosh(\omega x)+\cosh(\omega(1-x))-1-\cosh(\omega)\right)+\omega\left((1-x)\sinh(\omega x)+x\sinh(\omega(1-x))\right)\Big] \tag{39}$$

where we have made the substitution $4-6\beta \to 2+a$. Our goal is to show that $F_\omega(x) <= 0$ for any $\omega > 0$ and $x \in [0,1]$. We do this by confirming that $F_\omega(x)$ is convex in $(0,1)$, and that $F_\omega(0) = F_\omega(1) = 0$. Therefore by the maximum principle for subharmonic functions, $F_\omega(x) < 0$ on the interior $x \in (0,1)$.

To confirm convexity, we check that:

$$\begin{aligned}\frac{\partial^2 F_\omega}{\partial x^2} &= \omega^2\Big[\omega\left(x\sinh(\omega(1-x))+(1-x)\sinh(\omega x)\right)\\ &+ a\left(\cosh(\omega x)+\cosh(\omega(1-x))\right)\Big]\end{aligned} \tag{40}$$

The first term is positive; the second is positive if $a > 0$, which is true as long as $N > 10$. Checking that $F_\omega(0) = F_\omega(1) = 0$ is a simple matter of substituting $x = 0, 1$ into Eqn. (39).

In conclusion, we cannot make this network act as an integrator, by adjusting its Purkinje-to-vestibular connections. Instead, we would have to adjust the underlying vestibular-to-Purkinje projection pattern ϕ_1.

Figure 5 here

4 Example: The Rubinstein-Sternberg model

In this section we give a third, quite different, application for the technique based on low-rank perturbations. Rubinstein and Sternberg[2] introduced a nonlocal model for phase separation of the form

$$\begin{aligned} u_t &= \Delta u - f(u) - \frac{1}{|\Omega|}\int_\Omega f(u)dx \qquad (x,t) \in \Omega \times (0,\infty)\\ \mathbf{n}\cdot\nabla u &= 0 \qquad\qquad x \in \partial\Omega. \end{aligned}$$

As an example we compute the stability of a standing front type solution of a one-dimensional Rubinstein-Sternberg model.

$$u_t = u_{xx} + f(u) - \frac{1}{2L}\int_{-L}^{L} f(u)dx \qquad\qquad u_x(\pm L) = 0. \tag{41}$$

This equation always admits a constant solution and for sufficiently large widths it admits front type solutions. At $L = \frac{n\pi\sqrt{f'(0)}}{2}$ a bifurcation occurs giving rise to a solution containing n fronts. In the absence of the non-local term these front solutions are (for L finite) always unstable. The most unstable mode has a non-vanishing mean, so the instability is connected with non-conservation of mass. Rubinstein and Stern-

berg introduced the non-local term as a Lagrange multiplier to enforced mass conservation and remove this non-physical instability mechanism.

It is easy to see that, if u represents a stationary solution to Eqn. (41) then the linearized evolution equation is given by

$$v_t = v_{xx} + f'(u)v - \frac{1}{2L}\int_{-L}^{L} f'(u)v dx \qquad\qquad v_x(\pm L) = 0.$$

Again this takes the form of a rank-one perturbation of a self-adjoint operator, the form that we have considered throughout this paper.

The problem with a bistable cubic nonlinearity, $f(u) = u - u^3$,

$$u_t = u_{xx} + u - u^3 - \frac{1}{2L}\int_{-L}^{L}(u - u^3)dx \qquad\qquad u_x(\pm L) = 0$$

is the simplest and most natural from a physical perspective, and can be analyzed rather explicitly. Assuming $L > \frac{\pi}{2}$ there is a front solution which can be expressed in terms of elliptic functions[2]. After a simple rescaling ($u = (1+k^2)^{-1}v$, $x = (1+k^2)^{-1/2}y$, and $t = \frac{\sqrt{2}k}{\sqrt{1+k^2}}s$), the equation can be written in the form

$$u_t = u_{xx} + (1+k^2)u - 2k^2u^3 - \frac{1}{2K}\int_{-K(k)}^{K(k)}((1+k^2)u - 2k^2u^3)dx \qquad\qquad u_x(\pm K(k)) = 0. \tag{42}$$

Here the quantity $k \in (0,1)$ denotes the elliptic modulus and $K(k)$ denotes the complete elliptic integral of the first kind

$$K(k) = \int_0^1 \frac{dx}{\sqrt{(1-x^2)(1-k^2x^2)}} \in (\frac{\pi}{2}, \infty).$$

The elliptic modulus k is determined from L by the relation

$$\sqrt{1+k^2}K(k) = L.$$

The unperturbed problem now becomes

$$u_t = u_{xx} + (1+k^2)u - 2k^2u^3 \qquad\qquad u_x(\pm K(k)) = 0; \tag{43}$$

a well-known identity for elliptic functions states that a stationary solution to this equation is given by

$$u(x;k) = \mathrm{sn}(x,k)$$

where sn is the Jacobi elliptic sinus function.

Note that as the function $\mathrm{sn}(x,k)$ is odd the nonlocal term $\frac{1}{2K}\int_{-K(k)}^{K(k)}((1+k^2)u - 2k^2u^3)\,dx$ vanishes; thus, this function solves *both* the perturbed and unperturbed problem (i.e. both Eqn. (42) and Eqn. (43)). However, the non-local term changes the stability problem; we will find that the stability properties of the two problems are not the same.

[2]For fixed period L there is actually a one-parameter family of front solutions. The one given here has zero net mass and is the simplest.

Linearizing around the elliptic function solution gives the following linearized non-local evolution equation

$$v_t = v_{xx} + (1+k^2)v - 6k^2\mathrm{sn}^2(x,k)v - \frac{1}{2K(k)}\int_{-K(k)}^{K(k)}(1+k^2-6k^2\mathrm{sn}^2(x,k))v dx \tag{44}$$

$$= \mathbf{H}v - \frac{1}{2K(k)}\int_{-K(k)}^{K(k)}(1+k^2-6k^2\mathrm{sn}^2(x,k))v dx \tag{45}$$

$$= \tilde{\mathbf{H}}v \tag{46}$$

As in the other examples considered in this paper the linear operator $\tilde{\mathbf{H}}$ takes the form of a rank-one perturbation of a self-adjoint linear operator $\mathbf{H}$. The operator $\mathbf{H}$ is a two-gap Lamé operator, for which the spectral problem can be solved exactly [34, 35]. When subject to periodic boundary conditions on $[-2K(k), 2K(k)]$ the largest five eigenvalues are simple and are given by

$$\begin{array}{ll}
\phi_0^{(N)}(x) = k^2\mathrm{sn}^2(x,k) - \frac{1+k^2+a(k)}{3} & \lambda_0^{(N)} = -(1+k^2-2a(k)) \\
\phi_1^{(D)}(x) = \mathrm{cn}(x,k)\mathrm{dn}(x,k) & \lambda_1^{(D)} = 0 \\
\phi_1^{(N)}(x) = \mathrm{sn}(x,k)\mathrm{dn}(x,k) & \lambda_1^{(N)} = -3k^2 \\
\phi_2^{(D)}(x) = \mathrm{cn}(x,k)\mathrm{sn}(x,k) & \lambda_2^{(D)} = -3 \\
\phi_2^{(N)}(x) = k^2\mathrm{sn}^2(x,k) - \frac{1+k^2-a(k)}{3} & \lambda_2^{(N)} = -(1+k^2+2a(k))
\end{array} \tag{47}$$

with $a(k) = \sqrt{1-k^2+k^4}$. Here the superscript indicates whether the function satisfies a Neumann or a Dirichlet condition at $\pm K(k)$. Thus the unperturbed operator subject to Neumann boundary conditions has one positive eigenvalue $\lambda_0 = -(1+k^2-2a(k))$ and the remainder of the eigenvalues on the negative real line.

As noted above the stability problem (Eqn. (46), plus boundary conditions $v_x(\pm K(k)) = 0$) takes the form of a rank-one perturbation of a self-adjoint problem:

$$\tilde{\mathbf{H}}v = \mathbf{H}v + F\langle g, v\rangle$$

with $F = -\frac{1}{2K(k)}\mathbf{1}$ and $g = (1+k^2-6k^2\mathrm{sn}^2(x,k))$. While neither F nor g is an eigenvector of $\mathbf{H}$, the unperturbed operator, both F and g lie in the span of the zeroth and second eigenfunctions $\phi_{0/2}(x) = \phi_0^{(N)}(x) = k^2\mathrm{sn}^2(x,k) - \frac{1}{3}(1+k^2 \pm a(k))$. Since the eigenfunctions of a self-adjoint operator are orthogonal this implies that the rank-one piece, $F\langle g, v\rangle$ vanishes on the span of all the remaining eigenfunctions. This implies that the perturbed operator decomposes as a direct sum of two operators, one that is self-adjoint and negative definite and one that is rank-two:

$$\tilde{\mathbf{H}} \;=\; \underbrace{\tilde{\mathbf{H}}|_{\mathrm{span}(\phi_0,\phi_2)}}_{Rank-two} \oplus \underbrace{\tilde{\mathbf{H}}|_{\mathrm{span}(\phi_0,\phi_2)^\perp}}_{negative\ definite} = \tilde{\mathbf{H}}|_{\mathrm{span}(\phi_0,\phi_2)} \oplus \mathbf{H}|_{\mathrm{span}(\phi_0,\phi_2)^\perp}. \tag{48}$$

It is worth emphasizing that the perturbation term here is very special, in that F and g are actually given by linear combinations of just two of the eigenfunctions of the unperturbed operator. In the generic case (i.e. for a different nonlinearity $f(u)$) one expects F and g to have non-trivial projections onto all eigenfunctions.

From the exact eigenvalues in Eqn. (47) the second term satisfies the coercivity estimate

$$\tilde{\mathbf{H}}|_{\mathrm{span}(\phi_0,\phi_2)^\perp} \leq -3\mathbb{I}$$

and the entire stability problem is reduced to understanding the two by two matrix eigenvalue problem defined by $\tilde{\mathbf{H}}|_{\mathrm{span}(\phi_0,\phi_2)}$. Furthermore, since the range of $\tilde{\mathbf{H}}$ consists of mean zero functions it follows from the Fredholm alternative that $\tilde{\mathbf{H}}|_{\mathrm{span}(\phi_0,\phi_2)}$ must have a zero eigenvalue.

This zero eigenvalue is connected with mass conservation. There is a one-parameter family of solutions to this equation of fixed spatial period L, which can be thought of as being related to the total mass of the stationary solution. Here we have only considered the simplest solutions - those with zero net mass - but there are analogous expressions in terms of elliptic functions for the general solution. Since we have a one parameter family of solutions by Noethers theorem there must be an element in the kernel of linearized operator corresponding to the generator of this family.

It is straightforward to compute the restriction of the linearized operator $\tilde{\mathbf{H}}|_{\mathrm{span}(\phi_0,\phi_2)}$ in the (independent but non-orthogonal) basis $(1, \mathrm{sn}^2(x,k))$ in terms of complete elliptic integrals of the first and the second kind. By using the following identities

$$\begin{aligned} E(k) &= \textstyle\int_0^1 \frac{\sqrt{1-k^2x^2}dx}{\sqrt{1-x^2}} \\ \int_{-K(k)}^{K(k)} \mathrm{sn}^2(x,k)dx &= \tfrac{2(K(k)-E(k)}{k^2} \\ \int_{-K(k)}^{K(k)} \mathrm{sn}^4(x,k)dx &= \tfrac{(4+2k^2)K(k)-(4+4k^2)E(k)}{3k^4} \end{aligned}$$

one can derive the following expression for $\tilde{\mathbf{H}}|_{\mathrm{span}\phi_0,\phi_2}$, the restriction of the operator to the span of the zeroth and second eigenfunctions:

$$\tilde{\mathbf{H}}|_{\mathrm{span}\phi_0,\phi_2} = \begin{pmatrix} 6\frac{K(k)-E(k)}{K(k)} & \frac{3(1+k^2)(K(k)-E(k))}{k^2K(k)} \\ -6k^2 & -3(1+k^2) \end{pmatrix}.$$

Again we emphasize that this matrix representation is in the basis $\{1, \mathrm{sn}^2(x,k)\}$. The eigenvalues of this restriction are given by

$$\lambda_0 = 0 \tag{49}$$

$$\lambda_1 = \frac{(3-3k^2)K(k) - 6E(k)}{K(k)}. \tag{50}$$

It is easy to check directly from the definition of the elliptic integrals that the quantity $(3-3k^2)K(k) -$

$6E(k)$ is strictly negative for $k \in [0,1)$. This follows, for instance, from the Taylor series representations

$$K(k) = \frac{\pi}{2}\left(1 + \sum_{i=1}^{\infty}\left(\frac{(2i-1)!!}{(2i)!!}\right)^2 k^{2i}\right)$$
$$E(k) = \frac{\pi}{2}\left(1 - \sum_{i=1}^{\infty}\left(\frac{(2i-1)!!}{(2i)!!}\right)^2 \frac{k^{2i}}{2i-1}\right),$$

from which it is easy to see that the quantity $(1-k^2)K(k) - 2E(k)$ is even with only negative terms in its Taylor series, implying that it is strictly negative. Since the equation conserves mass it makes sense to consider only perturbations with zero net mass (those orthogonal to the kernel). In this case we have all eigenvalues strictly in the left half-plane and the stationary solution is non-linearly stable.

The problem for a general nonlinearity is slightly more complicated, since we do not have explicitly formulae for the eigenvalues and eigenfunctions, but it can essentially be completely solved. Assuming that the equation

$$u_t = u_{xx} + f(u) - \frac{1}{2L}\int_{-L}^{L} f(u)dx \qquad\qquad u_x(\pm L) = 0$$

has a stationary solution $u(x)$ we can compute the linearized operator as

$$\begin{aligned} \lambda v &= v_{xx} + f'(u)v - \frac{1}{2L}\int_{-L}^{L} f'(u)v\,dx, \qquad\qquad v_x(\pm L) = 0 \\ \Rightarrow \lambda v &= \mathbf{H}v - \frac{1}{2L}\langle f'(u), v\rangle \mathbf{1} = \tilde{\mathbf{H}}v \end{aligned}$$

where $\mathbf{H}$ is the unperturbed operator: $\mathbf{H}v = v_{xx} + f'(u)v$. It is convenient to introduce a coupling constant ρ controlling the strength of the perturbation, although we are mainly interested in the special case $\rho = 1$, and we thus consider a one-parameter family of eigenvalue problems

$$\tilde{\mathbf{H}}_\rho v = \mathbf{H}v - \frac{\rho}{2L}\langle f'(u), v\rangle \mathbf{1} = \lambda v$$

Applying the Aronszjan-Krein formula gives the following eigenvalue condition:

$$\begin{gathered} (\mathbf{H} - \lambda\mathbf{I})v = \tfrac{\rho}{2L}\langle f'(u), v\rangle \mathbf{1} \Rightarrow \\ v = \tfrac{\rho}{2L}(\mathbf{H} - \lambda\mathbf{I})^{-1}\mathbf{1}\langle f'(u), v\rangle \Rightarrow \\ \langle f'(u), v\rangle = \tfrac{\rho}{2L}\langle f'(u), (\mathbf{H} - \lambda\mathbf{I})^{-1}\mathbf{1}\rangle\langle f'(u), v\rangle. \end{gathered}$$

Thus the spectrum again decomposes into two pieces. Any eigenvectors of $\mathbf{H}$ which happen to be orthogonal to $f'(u)$ ($\langle f'(u), v\rangle = 0$) remain eigenvectors of the perturbed problem. Eigenvectors which are not orthogonal to $f'(u)$ must satisfy the eigenvalue condition

$$1 = \frac{\rho}{2L}\langle f'(u), (\mathbf{H} - \lambda\mathbf{I})^{-1}\mathbf{1}\rangle \tag{51}$$

Now note that one has the identity $\mathbf{H1} = f'(u)$ and thus we can write

$$\begin{aligned} 1 &= \frac{\rho}{2L}\langle \mathbf{H1}, (\mathbf{H}-\lambda\mathbf{I})^{-1}\mathbf{1}\rangle \\ &= \frac{\rho}{2L}\langle (\mathbf{H}-\lambda\mathbf{I}+\lambda\mathbf{I})\mathbf{1}, (\mathbf{H}-\lambda\mathbf{I})^{-1}\mathbf{1}\rangle \\ &= \rho + \frac{\rho}{2L}\langle \mathbf{1}\lambda, (\mathbf{H}-\lambda\mathbf{I})^{-1}\mathbf{1}\rangle \Rightarrow \\ &\Rightarrow \frac{\lambda}{2L}\langle \mathbf{1}, (\mathbf{H}-\lambda\mathbf{I})^{-1}\mathbf{1}\rangle - \frac{1-\rho}{\rho} = 0 \\ &\Rightarrow \frac{1}{2L}\sum \frac{\langle \mathbf{1}, v_i\rangle^2}{\lambda_i - \lambda} - \frac{1-\rho}{\rho\lambda} = h(\lambda) = 0 \end{aligned}$$

where we use the identity $\mathbf{1} = \sum\langle \mathbf{1}, v_i\rangle v_i$ and therefore that $(\mathbf{H}-\lambda\mathbf{I})^{-1}\mathbf{1} = \sum \frac{\langle \mathbf{1}, v_i\rangle}{\lambda_i - \lambda} v_i$; here, λ_i and v_i are the eigenvalues and (orthogonal) eigenvectors of the unperturbed operator $\mathbf{H}$. Notice that in the last expression $h(\lambda)$ is a Herglotz function — an analytic map of the open upper half-plane to itself — for $\rho \in (0, 1]$. It is well-known in scattering theory that diagonal matrix elements of the resolvent, such as the expression above, are Herglotz functions of the spectral parameter. This implies that the eigenvalues of the Rubinstein-Sternberg model for $\rho \in (0, 1]$ are real, since this function has a positive imaginary part in the upper half-plane: A complex eigenvalue would require $h(\lambda) = 0$ for some λ in the upper half plane.

This calculation shows that, despite the fact that the linearized operator is not self-adjoint, the spectrum is purely real for $\rho \in [0, 1]$. Now let us assume that we understand the spectrum of $\mathbf{H}_0 = \mathbf{H}$, the unperturbed operator, in particular that we know $n_+(\mathbf{H})$, the number of positive eigenvalues of the unperturbed operator. Let us consider doing a homotopy in the parameter ρ. Since we have shown that the eigenvalues are real the only way that an eigenvalue can move from the right half-plane to the left half-plane (or vice-versa) is by passing through the origin. We can detect when this occurs by taking $\lambda = 0$ in equation (51), which becomes

$$1 = \frac{\rho}{2L}\langle f'(u), \mathbf{H}^{-1}\mathbf{1}\rangle = \frac{\rho}{2L}\langle \mathbf{1}, \mathbf{1}\rangle = \rho$$

Here we have used the fact that $\mathbf{H1} = f'(u)$ so that $\mathbf{1} = \mathbf{H}^{-1}f'(u)$. (We are also assuming that $\mathbf{H}$, the unperturbed operator, is invertible. Minor changes are required in the case that $\mathbf{H}$ has a kernel; see Remark 1.) This calculation shows that the unique value of ρ for which $\mathbf{H}_\rho$ has a zero eigenvalue is $\rho = 1$.

We are now in a position to count the number of positive eigenvalues of $\tilde{\mathbf{H}}$ using a continuation argument. The operator $\tilde{\mathbf{H}}$ is bounded above and, by standard arguments, has a finite number of positive eigenvalues. We assume that the number of positive eigenvalues is given by $n_+(\tilde{\mathbf{H}}) = k$. At $\rho = 0$ there are k positive eigenvalues and the remaining eigenvalues are negative. For $\rho \in (0, 1)$ there kernel of $\tilde{\mathbf{H}}_\rho$ is empty, so no eigenvalues cross from the left half-line to the right. At $\rho = 1$ there is an eigenvalue at $\lambda = 0$, which either came from the left half-line or the right half-line. We can compute which via perturbation theory, by computing $\frac{d\lambda}{d\rho}$. Doing so we find that

$$\frac{d\lambda}{d\rho} = -\frac{2L}{\langle f'(u), \mathbf{H}^{-2}\mathbf{1}\rangle} = -\frac{2L}{\langle \mathbf{1}, \mathbf{H}^{-1}\mathbf{1}\rangle}.$$

If the quantity $\langle \mathbf{1}, \mathbf{H}^{-1}\mathbf{1}\rangle > 0$ the eigenvalue is moving from the positive half-line to the negative, while if $\langle \mathbf{1}, \mathbf{H}^{-1}\mathbf{1}\rangle < 0$ it is moving from the negative to the positive half-line. This proves the following theorem:

Theorem 1. *Suppose that the unperturbed operator* $\mathbf{H} = \partial_{xx} + f'(u)$ *is non-singular and has* $n_+(\mathbf{H}) = k$ *positive eigenvalues. The perturbed operator* $\tilde{\mathbf{H}}$ *has a simple kernel and* $n_+(\tilde{\mathbf{H}})$*, the number of positive eigenvalues of the linearized operator, is given by*

$$n_+(\tilde{\mathbf{H}}) = \begin{cases} k, & \langle \mathbf{1}, \mathbf{H}^{-1}\mathbf{1} \rangle < 0 \\ k-1, & \langle \mathbf{1}, \mathbf{H}^{-1}\mathbf{1} \rangle > 0 \end{cases}$$

Thus a necessary and sufficient condition for spectral stability is that $n_+(\mathbf{H}) = 0$ *(from which it follows that* $\langle \mathbf{1}, \mathbf{H}^{-1}\mathbf{1} \rangle < 0$*) or* $n_+(\mathbf{H}) = 1$ *and* $\langle \mathbf{1}, \mathbf{H}^{-1}\mathbf{1} \rangle > 0$*.*

Remark 1. *First we note that the case where the unperturbed operator* $\mathbf{H}$ *has a kernel can be addressed similarly. There one must do another perturbation calculation near* $\rho = 0$ *to understand how the zero eigenvalues move with* ρ *in order to compute* $n_+(\mathbf{H}_\rho)$ *for* ρ *small but non-zero. From there the calculation is the same: the number of positive eigenvalues can stay the same or decrease by one, and this is determined by the sign of* $\langle \mathbf{1}, \mathbf{H}^{-1}\mathbf{1} \rangle$*.*

We also note that, while this theorem requires some information on the spectrum of the unperturbed operator, the unperturbed operator is much nicer to deal with than the full linearization. The unperturbed operator is self-adjoint, so one has many more tools available to analyze it. Further the operator is actually of Sturm-Liouville type, so one can in principle compute the number of positive eigenvalues using Sturm oscillation theory.

5 Discussion

In conclusion, we have presented a general method of analyzing low-rank perturbations of self-adjoint operators. We show how to use a simple idea of classical differential geometry (the envelope of a family of curves) to completely analyze the spectrum. When the rank of the perturbation is two, this allows us to view the system in a geometric way through a "phase plane" in the perturbation strengths (ρ_1, ρ_2). By locating constant eigenvalue and eigenvalue coincidence curves (both computable through simple formulas), we can determine where the perturbed operator is stable, and where double real eigenvalues bifurcate into complex pairs. This latter situation (bifurcation into a complex pair) coincides with a poorly conditioned eigenvalue, which in turn signals that small changes in the perturbation parameter will yield large changes in the operator behavior.

We used these techniques to analyze three problems of this form; a model of the oculomotor integrator due to Anastasio and Gad[1], a continuum version of the oculomotor integrator model, and a nonlocal model of phase separation due to Rubinstein and Sternberg[2]. In the first two problems, the physical interpretation of our model (a neural network that must maintain a steady eye position in the absence of input) required that we identify (a) where the perturbed system had a specific eigenvalue and (b) where this particular eigenvalue would be poorly conditioned. Our results in §1 show that both (a) and (b) can only occur in proximity to a specific point on the (ρ_1, ρ_2) plane, which was then easy to visualize. In §2 and §3, some portions of the model are not completely specified by biology (such as the vestibular-to-Purkinje connections), but must be chosen arbitrarily (even randomly). In this paper, we analyzed a few carefully chosen examples. But, the geometric method we describe here also gives us rapid way to survey a large family of such models; using

such a survey to draw conclusions about the vestibular-to-cerebellar pathway is an area for future work.

In analyzing these three problems, we have by no means exhausted the possible applications. For example, the eigenvalue problem in Eqn. (29) is very similar to the stability problem for spike solutions to activator-inhibitor models in the limit of slow activator diffusion[3, 4] (although the problem we study here differs because the eigenvalue enters in a non-linear way). Similar models of reaction-diffusion equations with non-local interactions have arisen in a number of other contexts including population dynamics[36], runaway ohmic heating[5, 6, 7], microwave heating [8] and a reaction-diffusion equation with a global conservation of mass constraint[2]. Therefore, we anticipate that the techniques presented here should be applicable to understanding these problems.

Competing Interests

The authors have no competing interests.

Data Accessibility

Not applicable: the paper contains sufficient detail to reproduce the results.

Authors' Contributions

TJA, AKB, and JCB designed the project. TJA originated the integrator model described in §2; AKB and JCB originated the continuum integrator model (§3) and analyzed the Rubinstein-Sternberg model described in §4. AKB and JCB created figures; TJA, AKB and JCB wrote the paper.

References

[1] Anastasio TJ, Gad YP. Sparse cerebellar innervation can morph the dynamics of a model oculomotor neural integrator. Journal of Computational Neuroscience. 2007;22(3):239–254.

[2] Rubinstein J, Sternberg P. Nonlocal reaction-diffusion equations and nucleation. IMA J Appl Math. 1992;48(3):249–264.

[3] Freitas P. A Nonlocal Sturm-Liouville Eigenvalue Problem. Proceedings of the Royal Society of Edinburgh. 1994;124A:169–188.

[4] Iron D, Ward MJ. The dynamics of multispike solutions to the one-dimensional Gierer-Meinhardt model. SIAM J Appl Math. 2002;62(6):1924–1951 (electronic).

[5] Chafee N. The electric ballast resistor: homogeneous and nonhomogeneous equilibria. In: Nonlinear differential equations (Proc. Internat. Conf., Trento, 1980). New York: Academic Press; 1981. p. 97–127.

[6] Lacey AA. Thermal runaway in a non-local problem modelling Ohmic heating. I. Model derivation and some special cases. European J Appl Math. 1995;6(2):127–144.

[7] Lacey AA. Thermal runaway in a non-local problem modelling Ohmic heating. II. General proof of blow-up and asymptotics of runaway. European J Appl Math. 1995;6(3):201–224.

[8] Bose A, Kriegsmann GA. Stability of localized structures in non-local reaction-diffusion equations. Methods Appl Anal. 1998;5(4):351–366.

[9] Du Y, Hsu SB. On a Nonlocal Reaction-Diffusion Problem Arising from the Modeling of Phytoplankton Growth. SIAM J Math Anal. 2010;42(3):1305–1333.

[10] Bruce JW, Giblin PJ. Curves and Singularities. Cambridge University Press; 1984.

[11] Spivak M. Differential Geometry, Vol. III. 3rd ed. Publish or Perish; 1999.

[12] Robinson DA. Control of eye movements. In: Brooks VB, editor. Handbook of Physiology, Section 1: The Nervous System, Volume 2, Part 2. American Physiological Society; 1989. p. 1275–1320.

[13] Robinson DA. Integrating with neurons. Annu Rev Neurosci. 1989;12:33–45.

[14] Barreiro AK, Bronski JC, Anastasio TJ. Bifurcation theory explains waveform variability in a congenital eye movement disorder. Journal of Computational Neuroscience. 2009;26:321–329.

[15] Berthoz A, Jones GM. Adaptive Mechanisms in Gaze Control: Facts and Theories. Elsevier; 1985.

[16] Gonshor A, Jones JGM. Short-term adaptive changes in the human vestibulo-ocular reflex arc. Journal of Physiology. 1976;256:361–379.

[17] Gonshor A, Jones JGM. Extreme vestibulo-ocular adaptation induced by prolonged optical reversal of vision. Journal of Physiology. 1976;256:381–414.

[18] Tiliket C, Shelhamer M, Roberts D, Zee DS. Short term vestibulo-ocular reflex adaptation in humans. I. Effect on the ocular motor velocity-to-position neural integrator. Exp Brain Res. 1994;100:316–327.

[19] Cannon SC, Robinson DA, Shamma S. A Proposed Neural Network for the Integrator of the Oculomotor System. Biological Cybernetics. 1983;49:127–136.

[20] Robinson D. The effect of cerebellectomy on the cat's vestibuloocular integrator. Brain Res. 1974;71:195–207.

[21] Robinson DA. Adaptive gain control of vestibuloocular reflex by the cerebellum. Journal of Neurophysiology. 1976;39:954–969.

[22] Büttner-Ennever JA. Neuroanatomy of the Oculomotor System. Amsterdam: Elsevier; 1988.

[23] Zee S, Yamazaki A, Butler PH, Gücer G. Effects of ablation of flocculus and paraflocculus on eye movements in primate. J Neurophysiol. 1981;46:878–899.

[24] Chelazzi L, Ghirardi M, Rossi F, Strata P, Tempia F. Spontaneous saccades and gaze holding ability in the pigmented rat. II. Effects of localized cerebellar lesions. Eur J Neurosci. 1990;2:1085–1094.

[25] Rambold H, Churchland A, Selig Y, Jasmin L, Lisberger SG. Partial ablations of the flocculus and ventral paraflocculus in monkeys cause linked deficits in smooth pursuit eye movements and adaptive modification of the VOR. Journal of Neurophysiology. 2002;87:912–924.

[26] Nagao S, Kitazawa H. Effects of reversible shutdown of the monkey flocculus on the retention of adaptation of the horizontal vestibulo-ocular reflex. Neuroscience. 2003;118:954–969.

[27] Epema AH, Gerrits NM, Voogd J. Secondary vestibulocerebellar projections to the flocculus and uvulo-nodular lobule of the rabbit: A study using HRP and double fluorescent tracer techniques. Exp Brain Res. 1990;80:72–82.

[28] Langer T, Fuchs AF, Scudder CA, Chubb MC. Afferents to the flocculus of the cerebellum in the rhesus macaque as revealed by retrograde transport of horseradish peroxidase. J Comp Neurol. 1985;235:1–25.

[29] Langer T, Fuchs AF, Chubb MC, Scudder CA, Lisberger SG. Flocculuar efferents in the rhesus macaque as revealed by autoradiography and horseradish peroxidase. J Comp Neurol. 1985;235:26–37.

[30] Sekirnjak C, Vissel B, Bollinger J, Faulstich M, du Lac S. Purkinje cell synapses target physiologically unique brainstem neurons. J Neurosci. 2003;23:6392–6398.

[31] Tan H, Gerrits NM. Laterality in the vestibulo-cerebellar mossy fiber projection to flocculus and caudal vermis in the rabbit: A retrograde fluorescent double-labeling study. Neurosci. 1992;47:909–919.

[32] Babalian AL, Vidal PP. Floccular modulation of vestibuloocular pathways and cerebellum-related plasticity: an *in vitro* whole brain study. Journal of Neurophysiology. 2000;84:2514–2528.

[33] Keener JP. Principles of applied mathematics: transformation and approximation. Addison Wesley, Advanced Book Program; 1988.

[34] Magnus W, Winkler S. Hill's equation. Interscience Tracts in Pure and Applied Mathematics, No. 20. Interscience Publishers John Wiley & Sons New York-London-Sydney; 1966.

[35] Eastham MSP. The spectral theory of periodic differential equations. Texts in Mathematics (Edinburgh). Scottish Academic Press, Edinburgh; Hafner Press, New York; 1973.

[36] Furter J, Grinfeld M. Local vs. Nonlocal Interactions in Population Dynamics. Journal of Mathematical Biology. 1989;27:65–80.

Appendix

We fill in a few more details for calculating eigenvalues of:

$$\widetilde{\mathbf{M}}\vec{w} = \mathbf{M}\vec{w} + \rho_1 \vec{f}_1 \langle \vec{g}_1, \vec{w} \rangle + \rho_2 \vec{f}_2 \langle \vec{g}_2, \vec{w} \rangle = \lambda \vec{w}$$

First, act on this by the resolvent of the unperturbed operator, $R_\lambda = (\mathbf{M} - \lambda \mathbf{I})^{-1}$:

$$\begin{aligned} 0 &= (\mathbf{M} - \lambda \mathbf{I})\,\vec{w} + \rho_1 \vec{f_1}\langle \vec{g}_1, \vec{w}\rangle + \rho_2 \vec{f_2}\langle \vec{g}_2, \vec{w}\rangle \Rightarrow & (52)\\ R_\lambda\, 0 &= R_\lambda(\mathbf{M} - \lambda \mathbf{I})\vec{w} + \rho_1 R_\lambda \vec{f_1}\langle \vec{g}_1, \vec{w}\rangle + \rho_2 R_\lambda \vec{f_2}\langle \vec{g}_2, \vec{w}\rangle & (53)\\ 0 &= \vec{w} + \rho_1 R_\lambda \vec{f_1}\langle \vec{g}_1, \vec{w}\rangle + \rho_2 R_\lambda \vec{f_2}\langle \vec{g}_2, \vec{w}\rangle \Rightarrow & (54)\\ -\vec{w} &= \rho_1 R_\lambda \vec{f_1}\langle \vec{g}_1, \vec{w}\rangle + \rho_2 R_\lambda \vec{f_2}\langle \vec{g}_2, \vec{w}\rangle & (55) \end{aligned}$$

Now, act on the equation by both $\vec{g}_1$ and $\vec{g}_2$, to yield two consistency conditions:

$$\begin{aligned} -\langle \vec{g}_1, \vec{w}\rangle &= \rho_1 \langle \vec{g}_1, R_\lambda \vec{f_1}\rangle\langle \vec{g}_1, \vec{w}\rangle + \rho_2 \langle \vec{g}_1, R_\lambda \vec{f_2}\rangle\langle \vec{g}_2, \vec{w}\rangle & (56)\\ -\langle \vec{g}_2, \vec{w}\rangle &= \rho_1 \langle \vec{g}_2, R_\lambda \vec{f_1}\rangle\langle \vec{g}_1, \vec{w}\rangle + \rho_2 \langle \vec{g}_2, R_\lambda \vec{f_2}\rangle\langle \vec{g}_2, \vec{w}\rangle \Rightarrow & (57)\\ \langle \vec{g}_2, \vec{w}\rangle &= \frac{-\rho_1 \langle \vec{g}_2, R_\lambda \vec{f_1}\rangle\langle \vec{g}_1, \vec{w}\rangle}{1 + \rho_2 \langle \vec{g}_2, R_\lambda \vec{f_2}\rangle} & (58) \end{aligned}$$

Substituting Eqn. (58) into Eqn. (56) and dividing by the now common factor $\langle \vec{g}_1, \vec{w}\rangle$, will yield a single polynomial equation for ρ_1 and ρ_2:

$$0 = 1 + \rho_1 \langle \vec{g}_1, R_\lambda \vec{f_1}\rangle + \rho_2 \langle \vec{g}_2, R_\lambda \vec{f_2}\rangle + \rho_1\rho_2 \left(\langle \vec{g}_2, R_\lambda \vec{f_1}\rangle\langle \vec{g}_1, R_\lambda \vec{f_2}\rangle - \langle \vec{g}_1, R_\lambda \vec{f_1}\rangle\langle \vec{g}_2, R_\lambda \vec{f_2}\rangle \right) \quad (59)$$

When $\vec{g}_1 = \vec{g}_2$, the final $\rho_1\rho_2$ term is zero; this is what happens in the continuum example presented in §3.

We now explain how to apply this formalism to the eigenvalue problem in §3:

$$\beta\,(\Delta x)^2\,\psi_{xx} + (-1+3\beta)\psi + \frac{\rho_1\langle \psi, 1\rangle}{\Delta x(\lambda+1)}\delta(x-x_1) + \frac{\rho_2\langle \psi, 1\rangle}{\Delta x(\lambda+1)}\delta(x-x_2) = \lambda\psi, \quad \psi(0) = 0 = \psi(L) \quad (60)$$

Here, $\mathbf{M} = \beta\,(\Delta x)^2\,\psi_{xx} + (-1+3\beta)\psi$ and (as we expect negative eigenvalues) we will act on Eqn. (60) with the resolvent operator $R_\lambda \equiv \left(\beta\,(\Delta x)^2\,\psi_{xx} + (-1+3\beta)\psi - \lambda\psi\right)^{-1}$. Here $\vec{f_1} = \delta(x-x_1)$ and $\vec{f_2} = \delta(x-x_2)$; therefore $R_\lambda \vec{f_1}$ is equivalent to solving the Green's function problem

$$\beta\,(\Delta x)^2\,\psi_{xx} + (-1+3\beta)\psi - \lambda\psi = \delta(x-x_1)$$

Since ψ solves the PDE $\psi_{xx} + \frac{-1-\lambda+3\beta}{\beta\Delta x^2}\psi = 0$ for any $x \neq x_1, x_2$, ψ must have the following form:

$$\psi(x) = \begin{cases} A\sin\omega x, & x < x_1 \\ B\sin\omega x + C\cos\omega x, & x_1 < x < x_2 \\ D\sin(\omega(L-x)), & x > x_2 \end{cases}$$

where $\omega^2 = \frac{-1-\lambda+3\beta}{\beta(\Delta x)^2}$. By linearity of the resolvent, and the fact that $\vec{g}_1 = \vec{g}_2$, we can solve them together: i.e. $\rho_1\langle \vec{g}_1, R_\lambda \vec{f_1}\rangle + \rho_2\langle \vec{g}_2, R_\lambda \vec{f_2}\rangle = \rho_1\langle \vec{g}_1, R_\lambda \vec{f_1}\rangle + \rho_2\langle \vec{g}_1, R_\lambda \vec{f_2}\rangle = \langle \vec{g}_1, \rho_1 R_\lambda \vec{f_1} + \rho_2 R_\lambda \vec{f_2}\rangle = \langle \vec{g}_1, R_\lambda(\rho_1 \vec{f_1} + \rho_2 \vec{f_2})\rangle$.

Therefore we solve the Green's function problem only once; ψ must satisfy the following conditions, which

impose continuity of ψ at x_1, x_2 and the appropriate jump of the derivatives:

$$\begin{aligned}
\psi^+(x_1) &= \psi^-(x_1) && (61)\\
\psi^+(x_2) &= \psi^-(x_2) && (62)\\
\psi_x^+(x_1) - \psi_x^-(x_1) &= -\frac{\rho_1}{\beta(\Delta x)^3(\lambda+1)} = -\frac{\rho_1}{\beta^2(\Delta x)^3(3-(\Delta x)^2\omega^2)} && (63)\\
\psi_x^+(x_2) - \psi_x^-(x_2) &= -\frac{\rho_2}{\beta(\Delta x)^3(\lambda+1)} = -\frac{\rho_2}{\beta^2(\Delta x)^3(3-(\Delta x)^2\omega^2)} && (64)
\end{aligned}$$

This yields a system of 4 equations in the 4 unknowns A, B, C, and D. Similarly, we can express the action of $\vec{g}_1$ on any function of the form Eqn. (61) as a vector inner product: in this case,

$$\begin{aligned}
\langle 1, \psi\rangle &= \mathbf{g}^T\mathbf{w}, && (65)\\
\mathbf{g} &= \frac{1}{\omega}\begin{bmatrix} 1-\cos\omega x_1 \\ \cos\omega x_1 - \cos\omega x_2 \\ \sin\omega x_2 - \sin\omega x_1 \\ 1-\cos(\omega(L-x_2)) \end{bmatrix}; \qquad \mathbf{w} = \begin{bmatrix} A \\ B \\ C \\ D \end{bmatrix} && (66)
\end{aligned}$$

Thus our final polynomial is $0 = 1 + \mathbf{g}^T\mathbf{w}$, where $\mathbf{w}$ is the vector of coefficients we obtained by solving Eqn. (61–64).

We have final possibility; which is that $\lambda = -\alpha$; this corresponds to $\omega = 0$, or to a piecewise linear function (which is a general solution for $\psi_{xx} = 0$). We first note that by Eqns. (27), (28), such a solution must satisfy $\langle 1, \psi\rangle = 0$, or

$$\begin{aligned}
\langle 1, \psi\rangle &= \tilde{\mathbf{g}}^T\mathbf{w}, && (67)\\
\tilde{\mathbf{g}} &= \begin{bmatrix} x_1^2/2 \\ x_2 - x_1 \\ (x_2^2 - x_1^2)/2 \\ (L-x_2)^2/2 \end{bmatrix}; \qquad \mathbf{w} = \begin{bmatrix} A \\ B \\ C \\ D \end{bmatrix} && (68)
\end{aligned}$$

and $\mathbf{w}$ is constrained by imposing the boundary conditions Eqns. (61) – (64), but on the function

$$\psi(x) = \begin{cases} Ax, & x < x_1 \\ B + Cx, & x_1 < x < x_2 \\ D(L-x), & x > x_2 \end{cases}$$

We can check that is satisfied for a straight line through the origin; for the case we treated in §3 ($L = 1$, $x = 1/3$, $x = 1/2$), it is

$$\rho_1 = -\frac{9}{8}\rho_2$$

Indeed, we can check that for $\lambda = -\alpha$, Eqn. (9) is satisfied, indicating that the envelope equations fail to be uniquely satisfied at this point. This is a singular piece of the envelope curve, and so the real eigenvalue pair does not necessarily "split" as we cross this line.

Figures

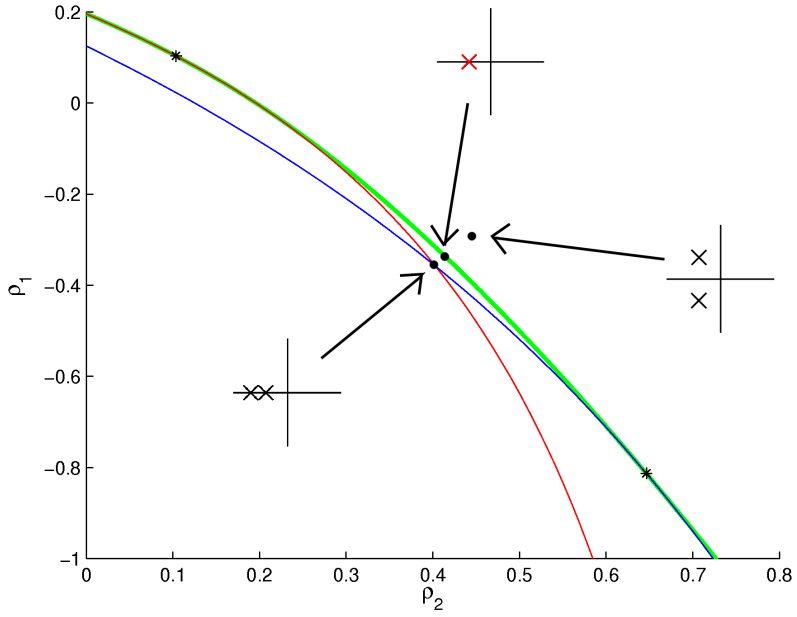

Figure 1: A schematic illustrating the bifurcation of eigenvalues across an envelope curve. The envelope curve (green bold solid) and two constant eigenvalue curves (blue and red light solid) are shown. The inset axes illustrate the relative positions of the eigenvalue pair in the vicinity of the bifurcation point.

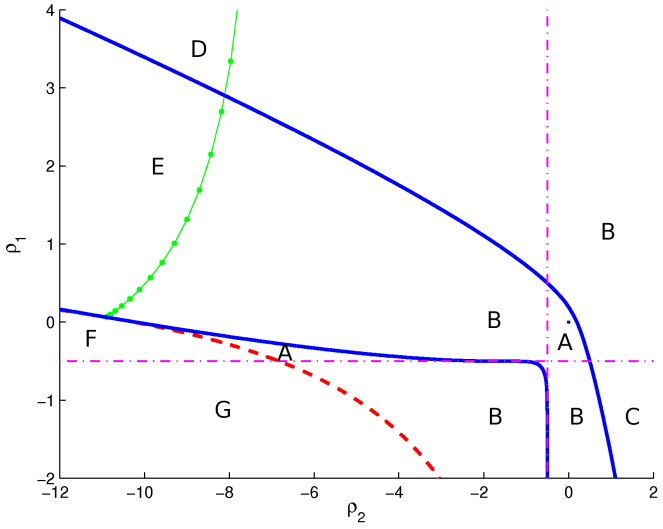

Figure 2: The stability diagram in the (ρ_2, ρ_1) plane for the model introduced in example 1. The bifurcation (blue), Hopf (green dotted), and zero eigenvalue (red dashed) curves are shown. The bifurcation curve also has a singular piece (magenta dot-dashed), for $\lambda = -2 + \frac{\sqrt{2}}{2}$, where the equations defining the envelope curve fail to have full rank.

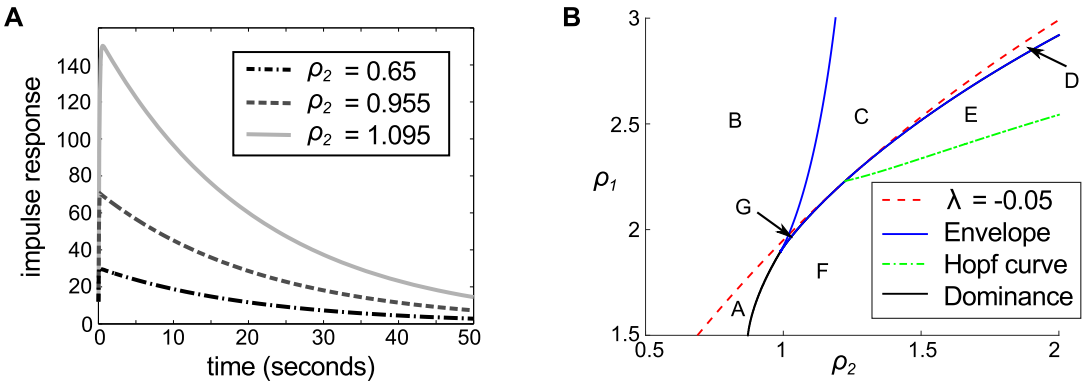

Figure 3: (A) Impulse response of network as network attempts to increase gain while maintaining $\lambda_{dominant}$. (B) Phase space of network showing normal operation. Letters indicate the relative positions of the *three* most dominant eigenvalues. Region A: 1 real (dominant), 2 complex in the LHP. Region B: 1 real (dominant) in the RHP, 2 complex in the LHP. Region C: 1 real (dominant) in the RHP, 2 real in the LHP. Region D: 2 real (dominant) in the RHP, 1 real in the LHP. Region E: 2 complex (dominant) RHP, 1 real LHP. Region F: 2 complex (dominant) LHP, 1 real LHP. Region G: 3 real LHP. We note that $\lambda_{dominant}$ is real unstable in B,C,D; complex unstable in E; complex stable in F; real stable in A,G.

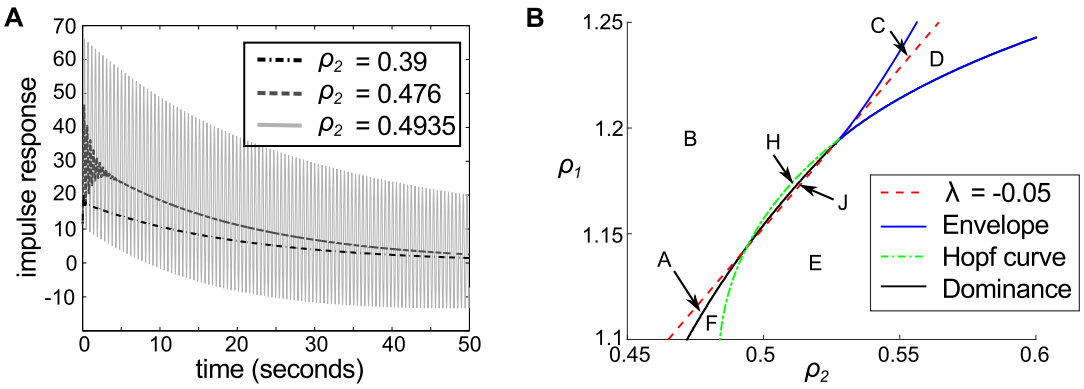

Figure 4: (A) Impulse response of network as network attempts to increase gain while maintaining $\lambda_{dominant}$. (B) Phase space of network showing pendular nystagmus. Letters indicate the relative positions of the *three* most dominant eigenvalues; labels are as in Fig. 3, with the addition of new regions "H" and "J". Region A: 1 real (dominant), 2 complex in the LHP. Region B: 1 real (dominant) in the RHP, 2 complex in the LHP. Region C: 1 real (dominant) in the RHP, 2 real in the LHP. Region D: 2 real (dominant) in the RHP, 1 real in the LHP. Region E: 2 complex (dominant) RHP, 1 real LHP. Region F: 2 complex (dominant) LHP, 1 real LHP. Region H: 1 real (dominant) and 2 complex in the RHP. Region J: 2 complex (dominant) and 1 real in the RHP. (There is no Region G: 3 real LHP here). We note that $\lambda_{dominant}$ is real unstable in B,C,D,H; complex unstable in E,J; complex stable in F; real stable in A.

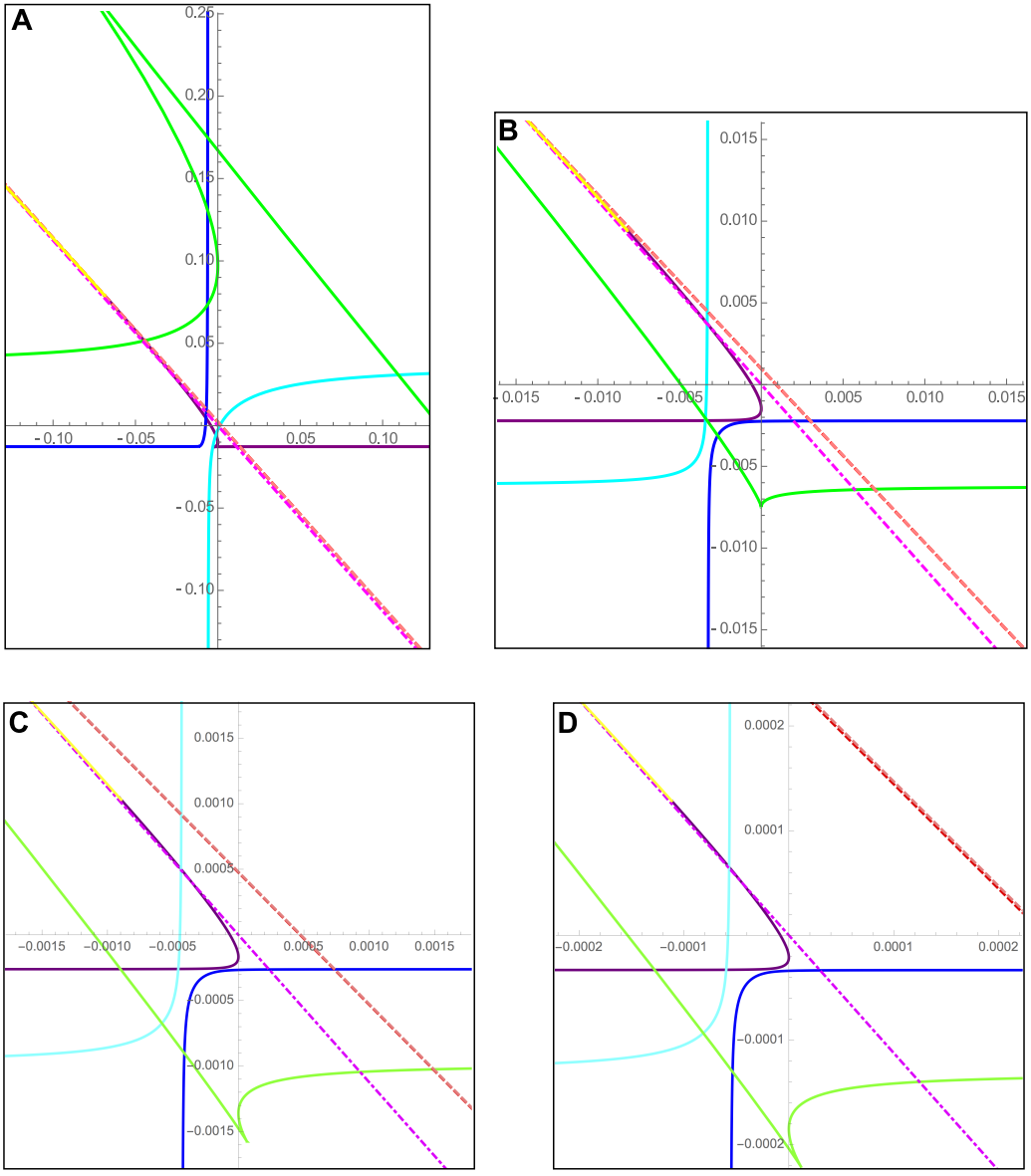

Figure 5: Phase planes for the continuum oculomotor integrator model (Eqn. (26–28)), for several values of N. Four pieces of the $\lambda < 0$ bifurcation curve are shown: $(0, 4\pi)$ (purple), $(4\pi, 6\pi)$ (blue), $(6\pi, 8\pi)$ (cyan), $(8\pi, 12\pi)$ (green); $\lambda > 0$ curve (yellow). The singular piece is also shown, corresponding to $\lambda = -1$ (magenta dot-dashed). Constant eigenvalue curves $\lambda = -0.05/200$ (red dashed) and $\lambda = 0$ (pink dashed) are visually indistinguishable. (A) $N = 12$. (B) $N = 24$. (C) $N = 50$. (D) $N = 100$.